Possible detection of tachyon monopoles in photographic emulsions

Keith A. Fredericks
Restframe Labs, W. Lafayette, IN 47906 USA
(Dated: June 7, 2013)

Certain experiments using photographic emulsions show unique particle tracks suggesting detection of magnetically charged particles with faster-than-light velocities. Particle kinetic energy is estimated from energy deposition and momentum is estimated from track curvature in magnetic fields. On a kinetic energy versus momentum graph, measured values for sample tracks fall in the $v > c$ region. Track curvature is parabolic, which is a signature for monopoles. The plane of curvature suggests electrically charged tachyons detected as slower-than-light monopoles. Particle mass and velocity were estimated. Further study is suggested to broaden this search.

CONTENTS

I. INTRODUCTION

A unique collection of particle track effects has been observed in a variety of studies[1–11] since 1979. The same track effects have been observed in diverse experiments including bombardment by low-energy ions in glow discharge plasma processes,[10,11] electric explosion of metallic wires and thin foils,[2,3,6] low-energy discharges in water,[4,5] the search for monopoles of solar origin at the north pole,[7] the supercompression of solid targets using electron beams,[8,9] and exposure to human hands.[1] All experiments cited here recorded particle tracks using

photographic emulsions except [8 and 9], which recorded tracks with MDS (metal-dielectric-semiconductor).

Kuznetsov, *et.al.*[12,13] reviewed and analyzed experiments by several of the authors above[2,3,9–11] and others where the so-called "strange radiation" was registered on photographic emulsions and metal surfaces. Kuznetsov, *et.al.* mainly discusses the reported transmutation phenomena, but does not go into detail on the nuclear track results.

Our experiments,[1] from 1979 observed track effects primarily under conditions where human fingertips were *exposed* to photographic emulsions. The use of amplified photographic emulsions in these experiments significantly enhanced the sensitivity to the track effects and facilitated the recording of a number of important effects not observed in other experiments and led to the most comprehensive collection of anomalous particle tracks.

The data generated in these experiments replicates very closely virtually all track effects observed in Refs. [2, 4–11]. With over 200 exposures and thousands of tracks on photographic film, we believe that our collection of data in this area is the largest and most extensive of all related studies with particle tracks. A comparison of data from these studies is included in Appendix B.

It must be noted that other studies (see *e.g.* references in [10]) detected similar anomalous tracks using photographic emulsions, but we believe our initial recognition of tracks in 1979 pre-dates all other studies.

First the experiments are briefly reviewed, the analysis of the data is extended and recommendations for future work are made.

A. Review of Experiments

1. Urutskoev, et.al.

Urutskoev, *et.al.*[2] searched for explanations of their observations of the apparent transmutation of elements in exploding wires and foils in "low-energy" nuclear reactions. During their experiments, they placed fluoroscopic, radiographic and nuclear track emulsions at a distance from the reaction vessel, or from samples of reaction by-products, and exposed the films at certain periods. They used applied magnetic fields of $B \sim 20G$ at the reaction site and at other times applied the magnetic field of a samarium-cobalt permanent magnet, $B \sim 1.2kG$ to the detector. They observed what they termed "strange radiation" on the emulsions and reported a number of types of tracks, or as they say, *traces* including *comets* and *caterpillar traces* and noted various properties of the tracks.
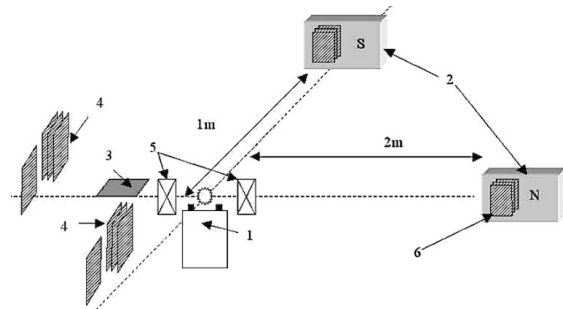

FIG. 1. Urutskoev, *et.al.* experimental setup. 1) site of electric explosion of foils, 2) permanent magnets 3) nuclear emulsion 4) emulsions 5) magnetic field coil 6) emulsions near permanent magnet. Diagram provided courtesy of L. Urutskoev.

Many tracks are characterized as "spirals and gratings." *One of the properties observed was that often a second, less-defined track would appear parallel to another more-defined track.* Urutskoev, *et.al.* also reported track width to vary with distance from the detector from $30\mu m$ to $5\mu m$ at a 2m distance.

One can also observe what appear to be very large-angle deflections or possibly the meeting of two particle tracks at a vertex.

Urutskoev and co-workers continued to analyze the data along with other collaborators and arrived at a hypothesis of a magnetically charged particle as responsible for the tracks. These researchers notably teamed with Georges Lochak to interpret the data as the result of Lochak monopoles.[14]

2. Ivoilov

Ivoilov, in a study[4] to further investigate the results of Urutskoev and co-workers used low-energy discharges in liquids and excitation of beta-decay products in magnetic fields.
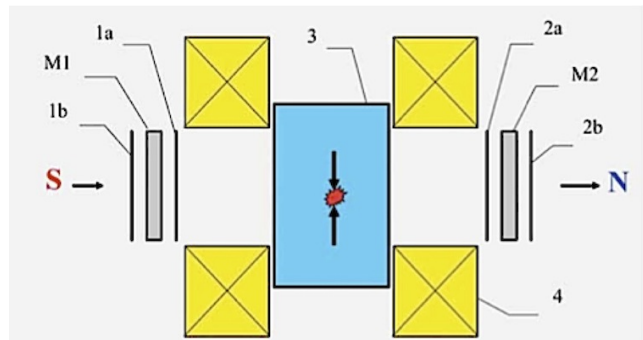

FIG. 2. Ivoilov experimental setup. 1,2) X-ray emulsions, M1,M2) the material investigated, 3) thin wall plastic vessel, 4) Helmholtz induction coils, S,N) magnetic field direction. Diagram provided courtesy of N. Ivoilov.

The experimental setup was surrounded at a distance of 10-15cm from the *source of the radiation.* Double-sided X-ray film was exposed for 3-10min. during the discharge. Ivoilov states that the results were *completely identical* to those of Urutskoev and co-workers.

Ivoilov observed pairs of tracks, with symmetry from an *inversion center* on opposite sides of the 2-sided X-ray film. In addition, *discrepencies were observed as the separation between these pairs changed.*

Ivoilov analyzed the results and proposed, in conjunction with Georges Lochak that the observations were due to the *Lochak* monopole[14] and further that the pairs of detected particles were *chirally symmetric.*

3. Rodionov and Savvatimova

Rodionov and Savvatimova[10] gave a brief review of experiments where particle tracks were observed on photographic emulsions and on surfaces of metal electrodes and showed a number of images they generated in experiments surrounding a glow discharge plasma with photographic emulsions and recorded images of the metal electrodes from the reaction vessel.
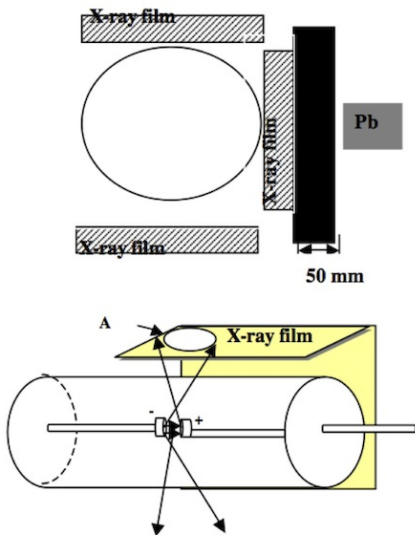

FIG. 3. Savvatimova-Rodionov experimental setup. Diagram provided courtesy of I. Savvatimova.

The general nature of the tracks is characterized in these studies as having widths usually about 10μm, lengths of millimeters and more, repeated patterns *like tire treads or necklaces, continuous lines, groups of lines and parallel lines.* It is noted that tracks differ from standard tracks left by heavy charged particles by their characteristic large-angle deflections and great lengths up to centimeters.

Several images are shown of tracks in palladium electrodes and in Kodak BioMax (autoradiographic emulsion), RT-2 X-ray, and nuclear track emulsions. These images show large-angle deflections or vertexes where two tracks co-terminate, and tracks with regular periodic structure, some of which are labeled as spirals.

4. Adamenko and Vysotskii

Adamenko and Vysotskii[8,9] use a method of supercompression of solids with a high-current vacuum tube diode leading to the apparent transformation of nuclei. In these experiments, the authors find macro-tracks of what they term ordered thermo-mechanical impact on the surfaces of MDS (metal-dielectric-semiconductor comprised of an Al-SiO$_2$-Si sandwich) targets. They find the tracks created in the MDS layers as *analogous* to the Urutskoev tracks in photographic emulsions.
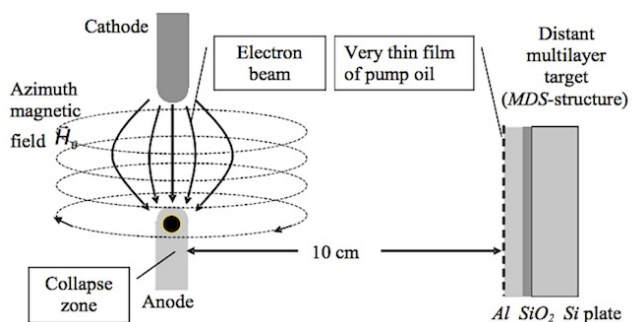

FIG. 4. Adamenko-Vysotskii experimental setup.

Total energy required for the formation of the track was calculated to be $\approx -10^6$GeV/cm. They note that this is 10^6 higher than the estimate made by Urutskoev, *et.al.*.[2] After analysis in the context of a magnetic charge, particle mass is estimated to be $\approx 10^{-23}g$ (≈ 560GeV). The authors suggest that the particle may fit within the framework of a magnetic monopole and more specifically the Lochak monopole.[14]

The particle track shown exhibits either a very large-angle deflection or the co-termination of two tracks. One half of the track shows a great deal of smooth curvature (much of which is parabolic). The very good micrographs give an unprecedented view of the almost perfectly correlated periodic structure of each part of the track leading up to the large-angle deflection. This track is analyzed in Appendix B and shown to agree in several respects with our analysis.

5. Priem, et.al.

Priem, *et.al.*[6,15] replicated the experiments of Urutskoev, *et.al.*[2] and found good agreement with their results related to both the by-products of the explosion of wires and the subsequent recording of particle tracks similar to Urutskoev, *et.al.*. The main things that stand out about this study are the photographic observations

of parabolic tracks (which are not noted as such, see Appendix B), tracks with regular periodic structure as in Urutskoev, *et.al.*[2] (see Section II G), and tracks with random or "irregular" structure (see Section II J). Each of these track types correspond to a specific track type in our study. Further detail and comparisons with similar tracks of our study are shown in Appendix B.

6. *Bardout,* et.al.

Bardout, *et.al.*[7] reported on the photographic results from an expedition to the north pole where a prediction of Georges Lochak was tested regarding the detection of monopoles traveling from the sun to the earth. Three tracks, exposed on Kodak Industrex MX125, are shown. The authors note that the tracks are similar to those detected in Urutskoev, *et.al.*. Large-angle deflections are seen in very long tracks with regular periodic[16] internal structure.

It is noted that one of the three tracks shown can also be interpreted as two co-terminating tracks, with one track nearly straight and the other exhibiting smooth curvature.

7. *Fredericks*

These experiments exposed human fingertips to emulsions for 2 to 30 min. and many experiments were carried out with an applied magnetic field perpendicular to the plane of the emulsion.

In these experiments, undertaken initially in the research laboratories of Rochester Institute of Technology Photographic Science department, a special photographic amplification technique was employed, making possible a higher level of photographic sensitivity specifically for line and dot images, greatly enhancing track visibility. See Appendix A for a complete description of this process.

Film type, amplification and development were analyzed. The tracks were observed on six different film types (Table I) using two different types of photographic development (Appendix A).

The effect was shown to occur independently of a dielectric isolator included between the fingertips and the photographic emulsion surface (Figs. 6 and 7).

Magnetic fields were applied during exposure using permanent magnets. Smooth, continuous track curvature was observed on certain exposures with applied magnetic fields and momentum was estimated between 2.7keV/c - 37keV/c *assuming circular curvature.*

In addition, strongly correlated tracks, numerous large-angle deflections, random motion tracks, and correlated random motion tracks were observed. A speculation of track formation via tachyons was put forth based on very long track lengths, random motion tracks and tracks with smooth curvature.

B. New Analysis

Fredericks[1] track data was re-examined microscopically using a Reichert Diapan and a Müller Researcher stereo microscope with a 14MP digital camera. Measurements of tracks were made using a stage micrometer and the ImageJ[17] program. Some tracks were digitally traced by hand using a vector graphics editor. Radius of curvature and angular measurements were done with the ImageJ system.

Particle tracks are analyzed and organized by properties such as width, length, curvature, structure, correlation and are shown in Section II.

A population of 18 specially selected *two-tailed* tracks with smooth curvature was evaluated. Curvature was found to be parabolic with a high degree of certainty with an average goodness-of-fit, $\overline{R}$-squared = 0.998. Results are shown in Section VII.

Particle momentum was estimated using the curved segments of the 18 specially selected two-tailed tracks. Average momentum in the two main models used was

1. Dirac tachyon monopole

   $\overline{p} \simeq 286.97\text{eV/c}$

2. Recami-Mignani tachyon monopole

   $\overline{p} \simeq 34.63\text{eV/c}$

Full results are shown in sections IV and VIII A.

Based on the measurement of widely varying track widths, the observation of track splitting (shown in Section II L), and a hypothesis that these particles can travel in bundles, a correction value, $\zeta = w/w_0$ (Section V) was applied to measured energy values versus measured track lengths.

Average $\zeta - corrected$ particle energy deposition is the same in both models:

1. Dirac and Recami-Mignani tachyon monopoles

   $\overline{E} \simeq 455.2\text{MeV}$

Full results are shown in Section III.

Using ζ-corrected measured momenta and kinetic energies, $\beta = v/c$ and mass were found using standard relativistic equations and transformed using a superluminal Lorentz transformation.

Graphical analysis of a kinetic energy vs. momentum graph yields $v > c$ for our sample particle tracks. Support is shown for the $v > c$ result as mass is *required* to be transformed using a superluminal Lorentz transformation. Average values (not to be confused with peak values used in Figs. 34 and 35) for mass, m' and β' are shown for two particle models (primed = superluminal Lorentz transformation)

1. Dirac tachyon monopoles

   $\overline{m}' \simeq$ -8.80×10^{5}GeV/c^2 : $\overline{\beta}' \simeq 2.12 \times 10^6$

2. Recami-Mignani tachyon monopoles

$$\overline{m}' \simeq \text{-}7.29{\times}10^6 \text{GeV}/c^2 \,:\, \overline{\beta}' \simeq 1.83 \times 10^7$$

Results of the tabulation of mass values were organized into a histogram and peak values were selected in Section VI A.

A subset of tracks in the current study is consistent with virtually all photographic nuclear track images produced in studies of "low-energy" (low-energy as in Low Energy Nuclear Reactions or LENR) electrical discharges and explosions in water using metal foils and electrodes,[2] low-energy electrical discharges in water and excitation of beta-decay products by magnetic fields,[4] bombardment by low-energy ions in glow discharge plasma processes,[10,11] and the search for solar magnetic monopoles at the north pole.[7] Data from these studies is compared side-by-side with our data in Appendix B.

C. Commentary

Bardout[7] and particularly Fredericks[1] stand out from the other studies due to the absence of any electrical explosions, discharges, their by-products or applied electric fields, which constitute in [2, 4–6, 8–11] the assumed source (or catalyst) of the phenomena. It is remarkable with these differences in exposure conditions that Fredericks duplicates virtually all observed track types. The only track type specifically *not observed* was the Ivoilov[4,5] "chiral" type track.

A relationship between all of the tracks in the present study is clearly established indicating a commonality of exposure, the mechanism of which is not clear.

The studies in Refs. [2, 4–6, 8, and 9] and analyses by Lochak[14,18] point to the *Lochak* monopole as responsible for these particle tracks.

The reasons cited for this are:

1. The particle that left the trace in the nuclear emulsion is charged, as nuclear emulsions are insensitive to neutrons.
2. The particle cannot have electric charge, as otherwise it could not be able to pass through two meters of atmospheric air and two layers of black paper.
3. The particle does not have high energy, as no delta-electrons are observed.
4. The mechanism of the interaction between the particle and the photosensitive layer is not clear. Assuming the Coulomb mechanism, the absorbed energy estimated using the darkening area equals around 1GeV.
5. The radiation is of nuclear origin; it interacts with magnetic fields.
6. Decomposition of ammonium nitrate, NH_4NO_3 by monopoles.
7. Enrichment of Uranium by monopoles.
8. β radioactive sample with an applied magnetic field produced the same particle tracks.
9. Reduction of β emitter half-life by monopoles.
10. Chirality of tracks exhibited with a Si or Ge reflector.
11. Biological effects where irradiation by monopoles stimulated the proliferation of bone marrow cells, increased resistance to genotoxic exposures, aggravated radiation disease, and changed cell composition in the blood.

Ivoilov also considers that some of the monopoles are magnetically excited neutrinos of cosmic origin[4] predicted by Lochak.[14]

Analysis by Lochak[14] of studies by Urutskoev[2] and Iviolov[4] indicated production of tracks by magnetic monopoles. Experiments and analysis by Adamenko and Vysotskii[8] regarding their own work and that of Urutskoev's also makes a case for magnetic monopoles.

These other studies are mentioned at various points throughout the text and summarized in Appendix B.

Tachyons, which were the subject of our earlier speculations, can be related to monopoles by a symmetry of Maxwell's equations and subject to an extension to the special theory of relativity. Using Lorentz transformations between superluminal and subluminal frames,[19–21] electrically charged tachyons turn into magnetically charged bradyons (slower than light particles) and vice-versa. In this interpretation[22,23] slower-than-light monopoles in subluminal frames are faster-than-light electrically charged particles in superluminal frames.

In addition, Lochak has presented nonlinear equations for tachyonic monopoles with mass.[14]

1. Source of Particles

It needs to be emphasized that the source of the particles is not at all clear.

Adamenko and Vysotskii[8] mention the possibility that either the particles were created in the laboratory with the electrical discharge *or* the particles are of cosmological origin.

Ivoilov[4] specified a *control background* of these tracks, [with origin] external to the laboratory, related to other observations with a laboratory *source*.

Bardout, *et.al.*[7], assumed that the source of particle tracks is the sun.

In the case of Fredericks, human fingertips contacted photographic emulsions but there is no evidence *and no claim* that this constitutes a source for the effect. In light of exposures by Fredericks with no fingertip contact and the collection of exposures in other studies with essentially identical particle tracks and *no fingertip contact*, it is possible that no exposure to fingertips is needed. Further experiments are needed to identify a source for the tracks.

The particles can be investigated without the identification of a source. For the moment questions about the source of the particles are set aside and the particle properties are investigated.

II. PHOTOGRAPHIC OBSERVATIONS

Visually[1] the tracks do not correspond with any of the tracks shown in reviews of photographic nuclear track studies[24,25] showing a wide variety of tracks of known particles such as electrons, protons, pions, nucleons, or alpha particles. Characteristics of ionizing particles such as delta rays are not seen (with one exception).[26]

Unlike electron tracks, these images are either continuous or with regular periodic structure and of nearly constant width. Unlike tracks of ions, the images show no delta-rays (a.k.a. the hairy rope). Unlike alpha particle tracks, these images are generally not straight lines and have been measured up to 69mm range in the emulsion plane (*cf.* particle type analysis of Lochak and Urutskoev[18]).

With respect to the sensitivity to magnetic deflection, the smoothness and length of these tracks in photographic emulsions more closely resembles tracks in bubble chamber or cloud chamber type detectors. The much longer tracks considered along with the relatively high density of photographic emulsions indicates that *normal* Coulomb scattering does not seem to play a role in track recording. This is a highly penetrating particle.

A. Experimental Technique

In total darkness, monodisperse (*i.e.* all grain sizes about the same) photographic emulsions, Kodak Kodalith Type III film or Kodak NTB3 nuclear track emulsions were given a uniform amplifying pre-exposure to light to increase photographic sensitivity.[27] One of three types of permanent magnets was placed with magnetic field, B perpendicular with the plane of the film (as shown in Fig. 5), on the sheet of film and the fingertips were placed on photographic film for an exposure time from 2 to 30 minutes. Then the film was processed using standard lith type (low-sulfite, hydroquinone) developer. In all of the experiments, great care was taken to assure proper handling, exposure and processing of the emulsions. (See Appendix A).

The track images occur independently of a clear plastic isolator to separate the hand from the emulsion. (See Figs. 6 and 7).

Using the exposure program mentioned earlier, under 8x to 22x magnification, track images are visible in the developed film in approximately 30-40% of exposures. Increasing the magnification range from 3.5x to 400x reveals a much higher percentage of tracks.

This search resembles the search for particles in modern particle search experiments in that data is generated and then scanned for events. (*cf.* [4] in the discussion of detection frequency.)
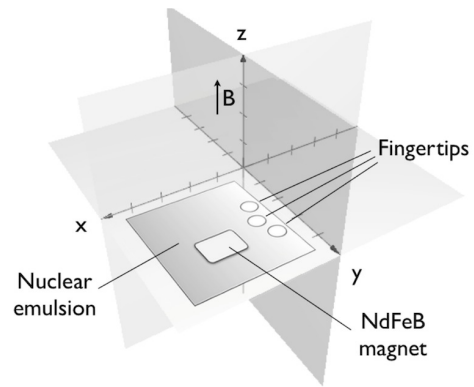

FIG. 5. Experimental setup of Fredericks showing M3, a neodymium permanent magnet.

FIG. 6. (1:2:R) Tracks in Kodalith type III film. The first exposure produced in 1979 showing recognizable tracks. A pre-exposure to diffuse tungsten light was given to a sheet of Kodak Kodalith Type III film. A plastic isolator (Saran^{TM}Wrap) covered the entire film surface and isolated the fingers from the photographic emulsion. The emulsion was exposed to the hand for a period of 25 minutes. The straight track on the right side appears to coincide with what we have seen of tracks of high-energy particles with delta-rays emanated along the track, but this is a reversed track. (See Fig. 10 and Section II H for overview and analysis of normal and reversed tracks).

Both positive and reversed tracks are observed. This is a purely photographic designation not based on observations of particle energy. Photons or electrons should create latent images on the AgBr crystals producing positive tracks, but the mechanism for reversed tracks requires additional study. However it is not totally unexpected that a reversal effect would result from a pre-exposed emulsion.
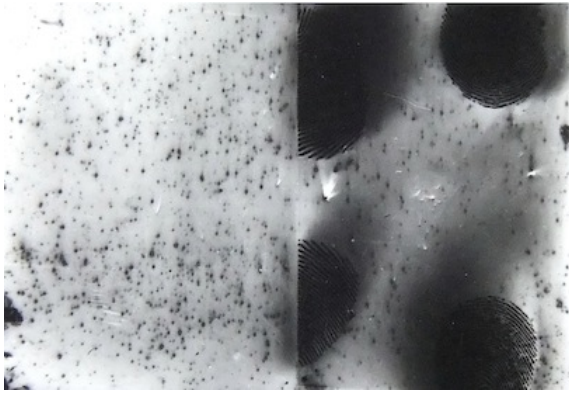
FIG. 7. (1:R) Image using NTB3 film, showing the effect of a dielectric isolator and the first three fingers of the left and right hands. The dielectric isolator, Saran^{TM}Wrap, covered the left half of the film, while the right half shows the direct exposure to fingertips. The general effect is to protect the film against fingerprints while allowing the particle track exposures.

Interestingly a third category of tracks we will refer to as "evaporated" are observed as track images apparently formed due to the absence of gelatin (or perhaps even plastic base). These tracks are normally only seen under magnification of $> 10x$ and are sometimes without Ag^0 (developed silver) being mostly clear except for the optical effects they produce.

B. Photographic Exposure and Development

The track effect has been observed on six different film types. The effect is most visible on film types Kodak NTB3 and Kodak Kodalith Type III using lith development. NTB3 is engineered to be electron sensitive and is generally sensitive to both ionizing and non-ionizing radiation from the visible part of the spectrum to gamma and beyond (with a cutoff in the hard UV to X-ray region due to absorption by gelatin). Both NTB3 and Kodalith Type III are monodisperse (all grains about the same size) emulsions. Other film types and development procedures also show the effect. Particularly interesting is the occurrence of tracks using both lith and solution physical development[28] using both monodisperse and polydisperse[29] emulsions.

Without magnification, most tracks are essentially invisible in monodisperse and polydisperse emulsions where agitation is used in development. Uniform pre-exposures and no agitation in development greatly enhances observation of the track images. Since agitation in development is the standard technique and high magnification is required to see many of the tracks, it is easy to imagine how these images have largely evaded recognition until now.

Lith development was used with and without agitation and solution physical development was used with agitation. A "border effect" is observed when a track intersects an area of high exposure. A uniform pre-exposure in conjunction with lith development with no agitation amplifies this photographic exposure effect with a photographic development effect called a border or edge effect,[30] greatly increasing the visibility of track images.

TABLE I. Observations of the track images under various conditions for various film types. PE=Pre-Exposure, Agi=Agitation

Film Type	Devel.	PE	Agi	Tracks
Polychrome Litho	lith		•	•
Kodak Plus-X	D-76		•	•
Kodak Kodalith	lith	•		•
Kodak NTB3	lith	•		•
Kodak Electronographic	lith	•		
Kodak Industrex	lith	•		•
Kodak Ektachrome	E-6		•	•

C. Image Formation

In the following we refer to the state of photographic development of the track image and the central track image in tracks with a border effect. Track images are formed on photographic film in one of three ways:

1. Type 1. Excitation of of the AgBr crystals via either ionization or light causing track images via developed AgBr crystals. This is referred to as "positive" or "normal exposure." This type of track image is seen on the emulsion as a dark line on a lighter background.
2. Type 2. Bleaching of the AgBr crystals via an unknown mechanism causing track images via the absence of developed crystals. This is referred to as "reversal" or "bleaching." This type of track image is seen on the emulsion as a white line on a darker background.
3. Type 3. Direct action on the gelatin and possibly the plastic base producing track images via the removal and/or deformation of plastic or gelatin. This is referred to as "evaporated." This category of track images can be clear, but visible due to the refraction of light and can also be accompanied by developed silver in the repeating patterns.

Some images are reversed for analysis. A reversed positive (type 1.) particle track image is generally seen as a white line on a darker background and a reversed (type 2.) particle track is seen as a black line on a lighter background.

Images are labeled in figures as to their type as above with (1),(2) and (3) and context with (O) for original, (R) for reversed. An image with both type 1 and type 2 tracks and reversed context is labeled as "(1:2:R)" and a type 1 track in original context is labeled "(1:O) See Figs. 9 and 10 for an overview of positive and reversed tracks and Section II H for a discussion of reversed tracks.

8

D. Lines and Dots

The tracks appear as dots and lines. Dots indicate an angle of incidence of the particle more perpendicular to the plane of the emulsion. Lines indicate an angle of incidence parallel to the plane of the emulsion.

Dots appear in various sizes, generally corresponding to track cross section dimensions. Some dots are substantially larger and some are "smeared." Some of these smeared tracks correspond to the *comet* tracks of Urutskoev, *et.al.*. (See Fig. 16a. in [2]).

Tracks often occur in "twin" pairs and corresponding groups of "nearly identical" tracks have also been identified.

E. Track Width

With an average grain size for Kodak NTB3 type emulsion of $0.34\mu m$ (undeveloped)[31] and an average AgBr/Gelatin ratio of 85%, assuming 100% of grains are developed, an average track cross section of $60\mu m$ may contain thousands of (AgBr) grains.

Track width has been measured to have a range of at least $5\mu m$ - $110\mu m$ (horizontal) and $5\mu m$ - $460\mu m$ (vertical).

Our track width measurements can be compared with studies by Urutskoev[2] using fluorographic, radiographic and nuclear emulsions and Iviolov[4] using a double-sided X-ray emulsion where $5\mu m$ to $30\mu m$ track widths were measured. These investigators also found that track width decreased as detector distance from the source was increased. It is noted also that in the Urutskoev and Ivoilov studies that both continuous and non-continuous tracks have been observed. See Appendix B.
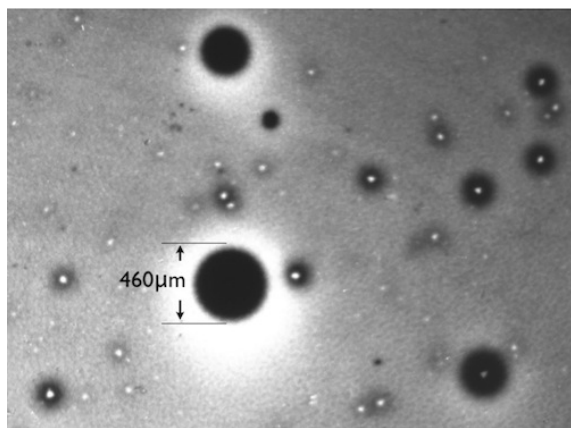

FIG. 8. (1:O) Micrograph at 25x of dots. Note the internal structure of all-black dots and dots with white centers. Kodak type NTB3 10μ emulsion.
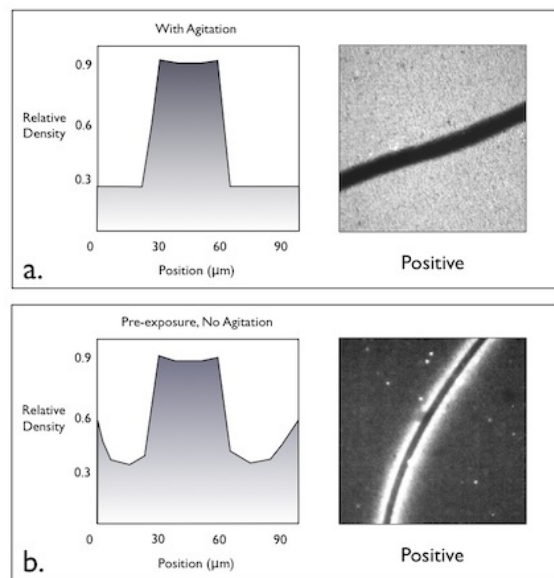

FIG. 9. Hypothetical microdensity profile across tracks showing a.) positive track with agitation during development. b.) positive track without agitation during development showing edge (adjacency) effect.
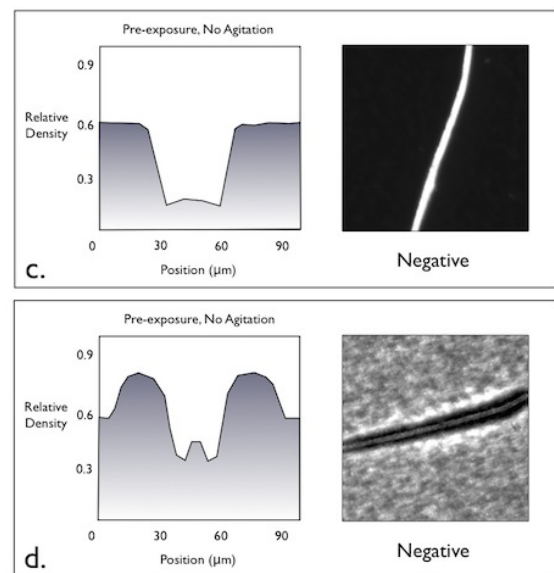

FIG. 10. Hypothetical microdensity profile across tracks showing c.) reversed track. d.) reversed track with edge effect.

In our studies, tracks have been observed with and without image amplification. In exposures with amplification, the inner track is surrounded by an edge, fringe or halo effect on both sides of the track. The white surround is a chemical adjacency effect.[30] With no agitation in development, the oxidation products of the developing agent hydroquinone build-up around the high exposure regions, affecting both size and density of high exposure

areas (border effect) and adjacent low exposure areas (halo effect). (See Fig. 9b). These effects in Fig. 10c and Fig. 10d are possibly due to additional exposure to light[30] or other radiation.

F. Track Length

Figs. 11 and 12 show a 69mm track. It is not clear if tracks have begun or ended in the emulsion. It is not immediately clear in what direction particles producing these tracks traveled although it may be possible to find track direction and charge by analyzing correlated pairs and groups of tracks in magnetic fields. This is the subject of future work. The tracks do not correspond to previously observed extensive cosmic ray tracks in photographic emulsions.[24,25]

There is tapering on both ends of the 69mm track. Since a specific type of tapering is expected for monopoles,[32] it may be of interest to analyze this tapering in detail.
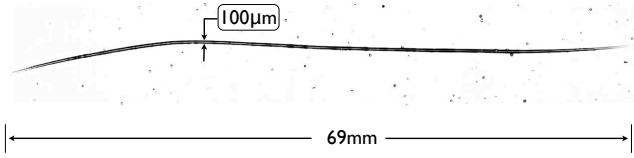
FIG. 11. (1:R) *69mm* track in Kodak NTB3 type emulsion. The track width average is 91μm.

FIG. 12. (1:R) Detail of 69mm track. Track structure of the internal saturated track surrounded by areas of local bleaching can be clearly seen. Each end of the track "fades," that is, the density of the central track image fades into the background as the local bleaching decreases and the track width decreases as well.

G. Regular Periodic Structure Tracks

Under magnification, tracks with regular periodic structure are seen. Certain tracks have a completely periodic structure whereas other tracks change in mid-track from wholly saturated tracks to periodic tracks (and possibly back to wholly saturated). Some totally saturated tracks show underlying periodic structure suggesting an intrinsic periodic track structure.
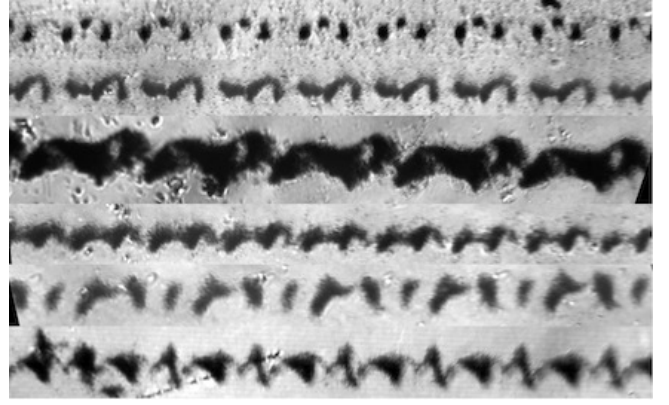
FIG. 13. (1:O) Different types of positive regular periodic structure tracks in Polychrome Litho film, no pre-exposure, developed with constant agitation.

Under low magnification, regular periodic structure tracks bear a closer resemblance to conventional charged particle tracks; yet possess a much greater track length than conventional particles *and* a regular periodic structure as opposed to the random nature[33] of grain patterns in conventional nuclear track studies.

FIG. 14. (3:O) Different types of "evaporated" regular periodic structure tracks in Polychrome Litho film, no pre-exposure, developed with constant agitation.

Under higher magnification, regular periodic structure tracks show specific repeated patterns. Others have called these patterns "beaded necklaces" and "caterpillars."
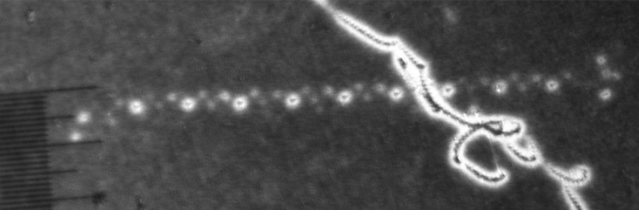
FIG. 15. (1:O) *Helical* Exposure shows a periodic pattern of dots *suggestive* of a helical track with 20μm width and an average inter-dot spacing (pitch) of 27.5μm. It is unclear however if this is (chaotic) helical motion or a repeated dot pattern as in Figs. 13 and 14. Polychrome Litho film, no pre-exposure, developed with constant agitation.

FIG. 18. (1:O) *Helical Hooks Detail* Detail of middle track w/inset showing structure. Topmost curve is exactly parabolic. Track width $= 30\mu$m. Polychrome Litho film, no pre-exposure, developed with constant agitation.

FIG. 16. (3:O) *zigzag* Exposure shows a periodic evaporated track in the form of a saw tooth at 400x magnification.

FIG. 19. (1:O) Patterned track. Kodak Industrex M (X-ray film) w/pre-exposure, developed with no agitation. Width $= 2.5\mu$m, Magnet $=$ M2.
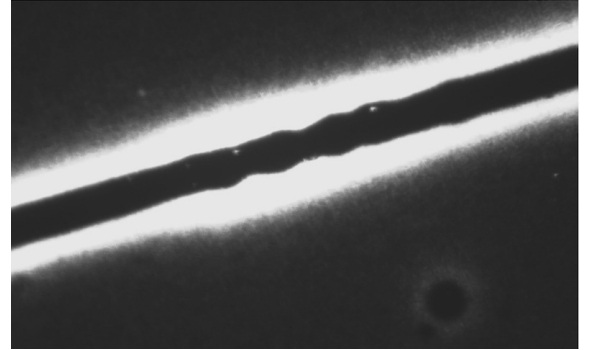
FIG. 20. (1:O) One of several areas of the 69mm track in Fig. 11 where the smooth-edged straight track changes to bumps on both sides of track indicating periodic and possibly helical motion. Track width $= 90\mu$m. Kodak NTB3 with pre-exposure, developed with no agitation.

The regular periodic structure is suggestive of helical trajectories or trajectories with some type of periodic, or possibly chaotic, spin component.
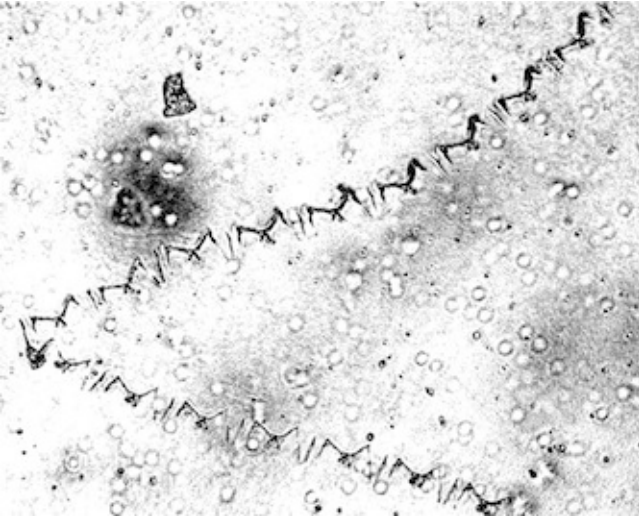

FIG. 17. (3:O) *spiral intersection* Exposure shows two periodic tracks meeting. This is an evaporated track with developed silver. 100x magnification.
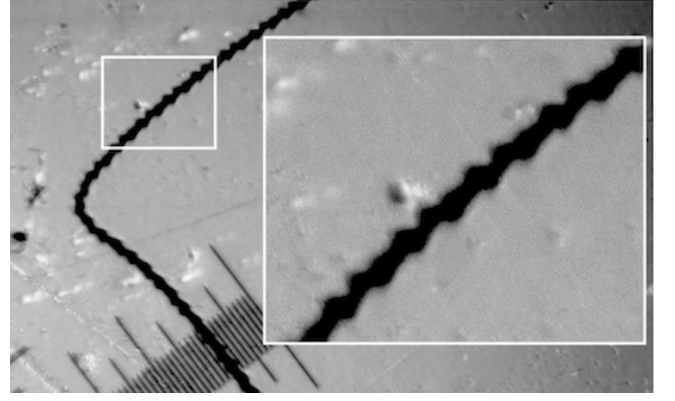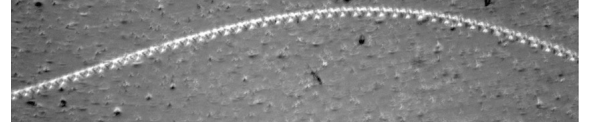
H. Reversed Tracks

Tracks can appear as either exposure (black, positive) or bleaching (white, reversed) The percentage of positive tracks versus reversed tracks has not been measured.

FIG. 21. (2:O) Photomicrograph of single track from Fig. 29, "Vector Swarm."

FIG. 22. (2:O) *hook*, Track 3 in Tables III, V - VII. Curved track in Kodalith type III film. Applied magnetic field of permanent magnet M3. a. raw track. b. Graph of parabola $x = y^2$ overlaid on track
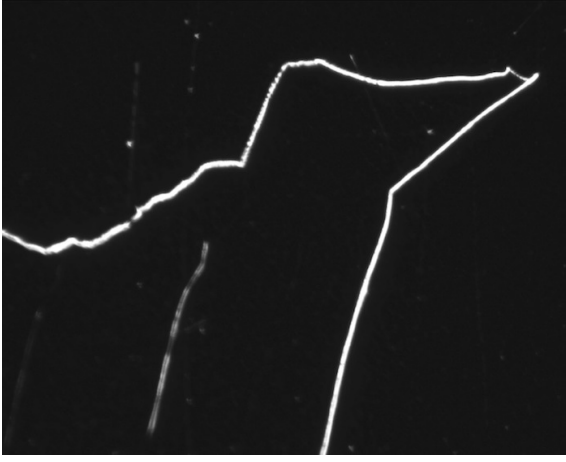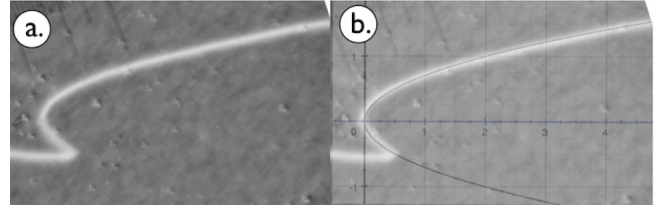
"Reversed" tracks appear to have formed due to a process that tears down or bleaches the latent image rather than a process that creates a developable latent image. Other examples of such tracks are shown in the middle right hand side of Fig. 6 and Figs. 28 and 29. In photographic processes where this type of bleaching occurs, the mechanism is probably a reversal effect caused by rehalogenation of the latent image.

In an AgBr photographic emulsion, the latent image, a region of Ag^0 metal forms as a result of exposure to light or ionizing radiation. In our case the initial exposure forming the latent image is the uniform pre-exposure to light. The Br^- ions, by-products of the latent image formation, still in solution in the gelatin, forms Br^0 in the region surrounding the latent image. With an additional exposure of the latent image to light or ionizing radiation, the Br^0 recombines with the Ag^0 due to the presence of positive holes, recreating non-developable, soluble AgBr grains.[30]

It is unclear exactly what causes two types of tracks, positive and reversed. Both positive and reversed tracks have been observed on the same exposure. The different tracks should be due to particles with different energy levels.

In virtually all exposures where a perpendicular magnetic field was applied with respect to the plane of the emulsion, track curvature is observed to be *exactly parabolic*. This can be seen visually in Figs. 22 and 23. Curve fitting, shown in Section VII using quadratic equations shows a near perfect fit to parabolas.

Curvature has also been observed with certain tracks to occur multiple times in different directions in the same track.
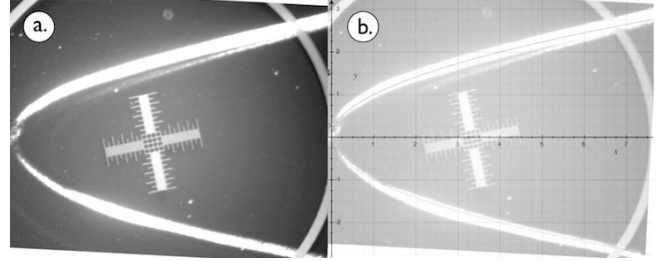
FIG. 23. (2:O) *loopy* Track length is 1.0cm. Magnetic field of M1. Kodak Kodalith type III emulsion. a. raw track with stage micrometer b. Graph of parabola $x = y^2$ overlaid on track

Particle momentum can be measured using tracks with smooth curvature. See Section IV, *Momentum Estimates from Track Curvature*.

J. Random Motion Tracks

Trajectories in Figs. 24 - 26 may correspond to the random or brownian motion of particles.
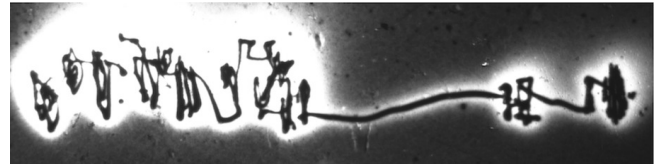
FIG. 24. (1:O) *squiggle2* Random motion type tracks in Kodak NTB3 10μ nuclear emulsion. Extreme large angle deflections and continuous smooth curvature are shown. Minimum track width = 10μm, track linear measure = 4.3mm.

I. Track Curvature

Photographic nuclear track studies commonly require magnetic fields at least 100 times greater than those used in cloud or bubble chamber work to produce measurable curvature in a photographic emulsion. The observations considered here indeed resemble tracks in bubble chambers more than tracks in photographic emulsions. This indicates highly penetrating particles and non-standard track exposure mechanisms.

FIG. 25. (1:O) *random1* Random motion type track in Kodak Kodalith Type III film. Extreme large angle deflections are shown.

FIG. 26. (1:O) *polysq* Random motion type tracks in Polychrome Litho emulsion. Extreme large angle deflections are shown.

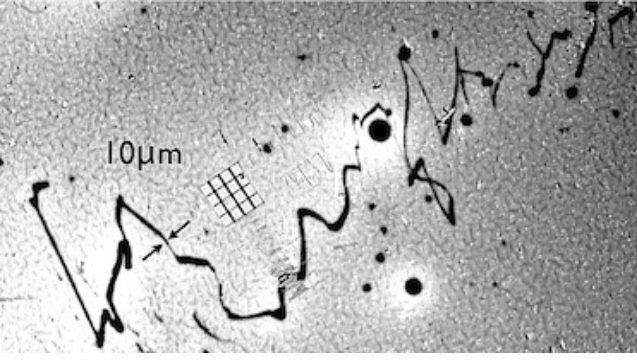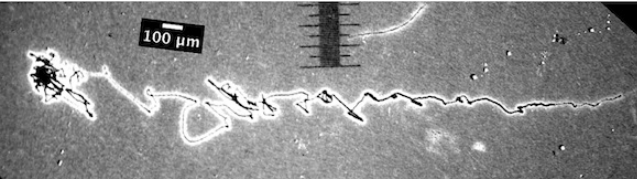Referring to the classic studies of particle tracks in nuclear emulsions based on detections of ionizing particles, large-angle deflections are very rare in photographic emulsions.[24] In these tracks, with linear measure up to $\sim 5mm$, large-angle deflections are numerous.

K. Correlated Tracks

Correlated trajectories and correlated random motion trajectories have not been seen in any of the standard photographic nuclear track studies done to date.
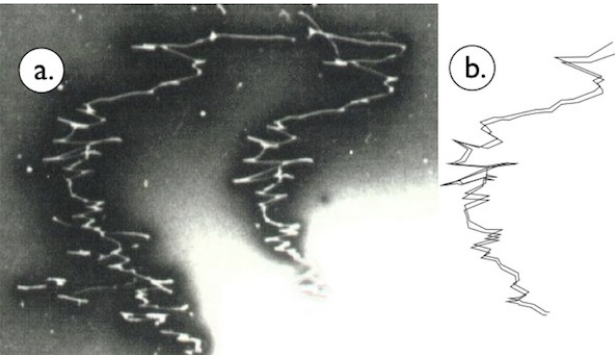

FIG. 27. (1:R) a.) Correlated random motion trajectories. Kodak 10μ NTB3 emulsion. b.) Using a graphics editor, the tracks were traced from the original. The tracks when superimposed upon each other reveal very similar though not quite identical structure.

However, we see correlated trajectories in the study by Ivoilov[4] with analysis by Lochak.[14]

Correlation of our tracks seems to be the rule and not the exception. Many particles appear to travel in pairs, shown in the analysis as tracks with a very high degree of correlation, even in the case of extremely complex trajectories.
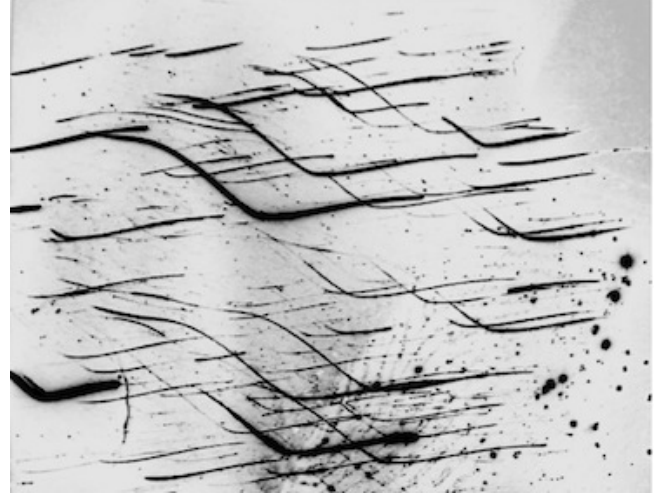
FIG. 28. (2:R) *Curve Swarm* Group of correlated tracks exhibiting smooth curvature. Note that tracks curve in both directions. Note also that these are white tracks on a black background. That is, these tracks are formed by a tearing down or bleaching of the latent image. A charged particle in an applied magnetic field (and no other applied fields) is expected to curve in only one direction according to the sign of its charge.

Particles found to be correlated throughout each of their trajectories appear to be connected. It is tempting to view this condition as a correlated particle experiment with the correlated tracks a visualization of entanglement.

In addition to observations of tracks in pairs, tracks in groups are also seen. It has emerged as a general rule in the scanning of these images, to look for twins. It is often likely that a twin image will be found. Many of these types of occurrences on earlier data were not seen, but with the recognition of dual and multiple tracks, it is now one of the first things to search for.

If a permanent magnet is used in the experiment, it is likely that correlated groups of tracks will appear.

Turning to Fig. 29, a very interesting region of track exposures was found. As with certain of the previous exposures, correlation of track images was seen. But instead of an entire group of carbon copies, we see a field of complex track structures with the same set of line segments, but each set of line segments has its own unique individual geometric transformation.

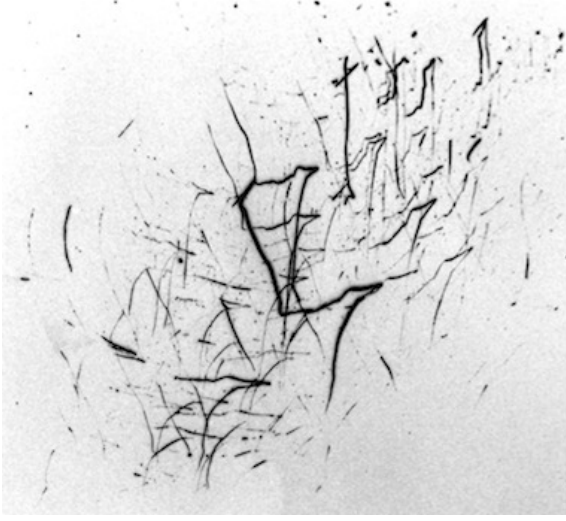FIG. 29. (2:R) *Vector Swarm* Group correlation of tracks including random motion components. Note similarity to Fig. 28. Note also that these too are tracks due to tearing down or bleaching of the latent image. Essentially identical track images such as Fig. 28 match when overlaid, but these tracks do not line up when overlaid. They change form with location, apparently due to relative position in the applied non-uniform magnetic field. A large number of the tracks in this exposure are correlated. A measure of corresponding line segments of matching groups of tracks reveals a macroscopic "central force" which will be the subject of future work.

The group of track exposures appears to be subject to a central force.

Correlated track images suggest correlation in time, space, and direction. Correlated groups of tracks certainly suggests that very similar particles are hitting the emulsion at the same time. Particles that are correlated must have a common history, presumably having undergone decay (splitting) at some time prior to hitting the emulsion.

If the correlation arises from the decay of an initial particle, (or *bundle* of particles) $X \rightarrow X + X$ ($2X \rightarrow X + X$), then the correlation we are seeing here should be non-classical and each of the particles with common origin should be entangled.

This image shows conclusive evidence of a real particle effect and what can only be a group of "identical correlated particles going through a series of quantum transitions in a non-uniform magnetic field.

L. Track Bundles

Tracks with internal structure and large measured widths are observed to apparently split in places.

In light of this, it is postulated that these particles can travel in bundles and that they can undergo various transitions such as splitting into correlated twins or swarms. Lower energy particles may be the result of the splitting of the higher energy bundle.
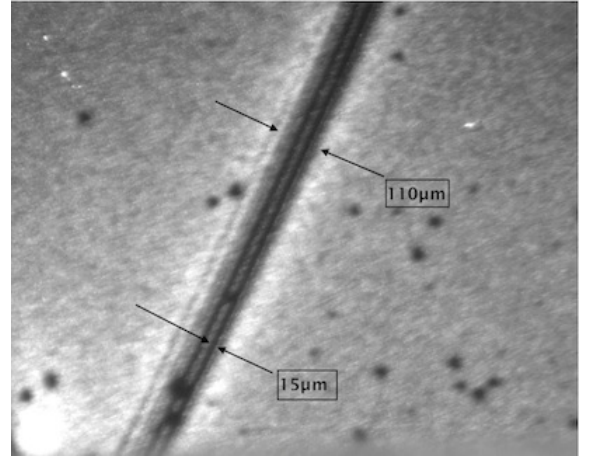
FIG. 30. (1:O) *Sub Tracks Detail* Micrograph at 45x magnification showing sub-track structure of the track bundle.

FIG. 31. (2:O) *bundle one* Track appears to be splitting into sub-tracks. Micrograph at 7x magnification. Kodalith Ortho type III film using permanent magnet M1.
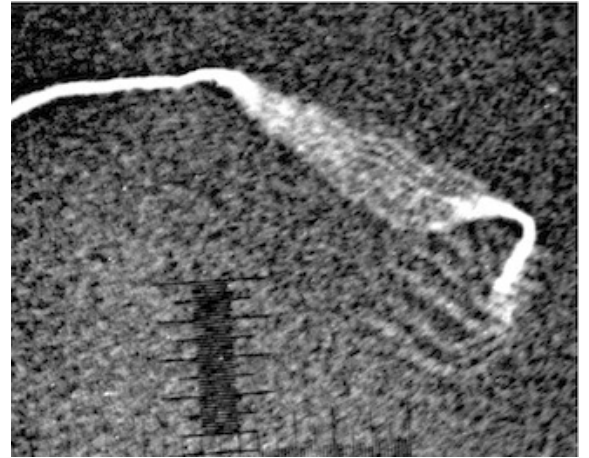

FIG. 32. (2:O) *Splitting* These types of tracks show splitting, reforming, and then splitting again. Kodalith Ortho type III film using permanent magnet M2.

The large 460μm round dot in Fig. 8 may be a very large vertically incident bundle of particles. Likewise, tracks that appear like smeared ink blots (reported in [2] and elsewhere) may be bundles in various states of splitting.

The result of Urutskoev, *et.al.* where they observed larger tracks closer to the source and smaller tracks at a further distance from the source may indicate that decay and splitting occurs for these particles over a one meter distance reducing a 30μm track to a 5μm track. It is noted that Urutskoev, *et.al.* mentioned[2] the idea that certain of the "ink blot" style tracks may be modeled as particle "clusters."

If the particles are traveling in bundles, a computation of particle energy or mass needs correction with respect to the base particle mass. One way to do this correction is shown in Section V.

M. Vertexes

In the set of all tracks, several types of vertexes are observed, but one type of vertex stands out. This is the two-tailed vertex.

Of particular interest is where one of the track segments is curved and the other is straight. These structures are either singular or infrequent in long tracks. They very often have similar features and are seen in either *concave* or *convex* configurations. These types of vertexes have been observed also in other studies [2, 4, 5, 7–11] and some are shown in Appendix B.
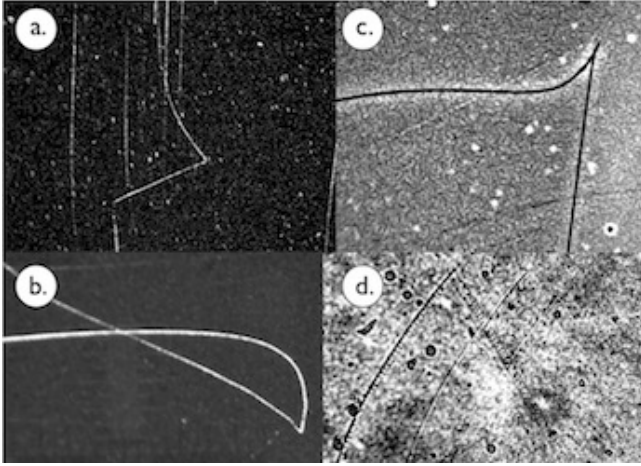

FIG. 33. a.) (2:O) One of a series of tracks with progressive curvature. Concave reversed track. Exact fit to parabola b.) (2:O) The classic vertex form. Convex positive track. Exact fit to parabola c.) (2:O) The concave form of the vertex. Reversed track. Exact fit to parabola d.) (3:O) Small convex form track using 400x magnification. Evaporated track. Exact fit to parabola.

Eighteen of these *two-tailed* tracks were selected for energy deposition and track curvature measurements and are the subject of analysis in Sections III - VIII A.

III. ENERGY LOSS

Observed properties of the tracks are used as a guide. The total energy deposited in the emulsion and the momentum estimates are used to evaluate expressions for the energy loss. What is known:

1. The particles interact with the photographic emulsion to leave tracks
2. Long (up to 69mm) track lengths in photographic emulsions indicate high energy and/or very penetrating particles
3. The particles travel in smoothly curving parabolic paths in a perpendicular applied magnetic field, but in the x, y plane rather than the x, z plane which would indicate magnetic monopoles
4. Large-angle deflections or co-terminations are observed
5. Smooth-saturated tracks are observed
6. Periodic structure tracks are observed
7. Random motion tracks are observed
8. Large variations in track width have been measured from $\sim 5\mu$m to 110μm (horizontal incidence) and $\sim 5\mu$m to 460μm (vertical incidence)
9. Tracks are observed to split
10. Multiple (many nearly exact) copies of tracks are observed
11. Properties are shared over different observations indicating a single particle type observed in various modes

These preliminary observations indicate an entirely new type of particle.

A. Deposited Energy

The energy loss in the emulsion is computed based on the number of developed (or bleached) AgBr grains.

A cylindrical track of length L has a volume $V = \pi r^2 L$ where r = radius of the cylinder. The right tail of the right-hand track in Fig. 43 will be used throughout as an example. We measure track length to be 13.3mm and track width to be 20μm or 0.02mm, so track radius, r = 0.01mm. Grain size (undeveloped), s_{grain} is 0.34μm[34] (developed grain size is about 70% of the undeveloped grain size[35] or 0.24μm) Shrinkage of the emulsion is neglected here since our tracks are horizontal and mostly saturated in a thin emulsion on a plastic base.[36]

$$V = \pi(0.01mm)^2(13.3mm) = 0.0042mm^3$$

The emulsion is undeveloped when it is exposed to the particles. The number of grains is estimated by computing the length of a cylinder of radius $r = s_{grain}/2$ where

s_{grain} = grain size. So, $r = 0.00017$mm and the length of a 0.34μm diameter cylinder is

$$L = \frac{V}{\pi r^2} = \frac{0.0042mm^3}{\pi(0.00017)^2mm} = 4.6 \times 10^4 mm$$

so

$$N_{grains} = \frac{L}{s_{grain}} = \frac{4.6 \times 10^4 mm}{0.00034mm} = 1.4 \times 10^8 mm$$

An AgBr/gelatin ratio of 85% in Kodak NTB3 emulsion[31] and Kodak Kodalith Ortho type III film is specified (although Kodalith would be lower) and this gives

$$N_{grains} = (1.35 \times 10^8)(0.85) = 1.15 \times 10^8$$

Due to the 10μm thickness of the emulsion, part of the 10μm track radius cylinder is outside of the emulsion, but that does not affect our result. Total energy within the cylinder is calculated. Part of the cylinder is just not registered by the emulsion.

B. Generalized Model

The tracks are observed in the gelatin, between the gelatin/air interface and the gelatin/plastic base interface and can be easily be observed at different depths between these interfaces using a microscope at 100x (or more) magnification.

The creation of tracks via *standard* ionization, excitation, or collision type mechanisms does not appear likely based on the observations, *i.e.* absence of delta-rays, periodic tracks, a large percentage of saturated tracks, many large-angle deflections, very long ranges up to 69mm, and (horizontal, *i.e.* in the plane of the emulsion) track widths up to 110μm (vertically incident track widths to 460μm).

Although none of these observations rules out the non-radiative mechanisms, it should be possible to rule it out for all known charged particle types in photographic emulsions based on classic studies of particle tracks.[24,25]

We choose here to generalize the energy loss computation for any mechanism by considering the energy required per grain to become developable in a photographic emulsion.

Katz and Kobetich[35] show that 63% of grains in an emulsion are developed when the energy is between 230 and 400eV/grain. For our purposes here, it is estimated that ∼90% of grains would be developed at a minimum of ∼600eV/grain producing a saturated track after our uniform pre-exposure energy of ∼150eV/grain. In this model a track exposure of 600eV/grain creates a saturated track.

This is a preliminary simplified model of energy level per grain where it is assumed that energy loss is the same at all values of β and energy loss is based on ionization. This can be improved in the future to better reflect

known energy losses at different values of β and by including various energy loss levels. Our example track is comprised of

$$(1.15 \times 10^8 grains)(600eV/grain) = 6.9 \times 10^{10} eV, \quad (1)$$

and in general energy loss per unit path or linear stopping power is

$$\begin{aligned} S_{linear} = \frac{dE}{dx} &= \frac{6.9 \times 10^{10} eV}{1.33cm} = 5.187 \times 10^{10} eV/cm \\ &= 51.87 GeV/cm, \quad (2) \end{aligned}$$

and with density, ρ of AgBr photographic emulsions[37] at 3.82 g/cm^3, mass stopping power is

$$\begin{aligned} S_{mass} = \frac{dE/dx}{\rho} &= \frac{5.187 \times 10^{10} eV/cm}{3.82 g/cm^3} \\ &= 1.36 \times 10^{10} eV\ cm^2/g \\ &= 13.6 GeV\ cm^2/g \quad (3) \end{aligned}$$

TABLE II. Linear stopping power based on the general model, measured values of number of grains, N_{grains} and track length, L for sample tracks.

Track	$S(GeV/cm)$	N_{grains}	L(cm)
"69mm" 11	1051.0	1.2×10^{10}	6.90
"67mm"	467.1	5.2×10^9	6.74
"hyper"	168.2	8.7×10^8	3.10
"short rev"	116.8	1.2×10^8	0.61
"rev caterpillar"	81.1	1.6×10^7	0.12
"bobby pins" 43	51.9	1.2×10^8	1.33
"curve swarm" 28	29.2	1.7×10^7	0.35
"birds"	13.0	5.2×10^6	0.24

IV. MOMENTUM ESTIMATES FROM TRACK CURVATURE

Tracks appear in photographic emulsions much like they would be expected to appear in a bubble chamber, often with long ($> cm$) track lengths and smooth curvature in magnetic fields, so it is straightforward to make track curvature measurements on the tracks as is done for bubble chamber photographs.

Initially it was thought that the curvature of these tracks was circular. (This error was also made in Ref. [6], see Appendix B). Upon closer inspection, the tracks can be seen visually Figs. 22 and 23 to correspond with a very high degree of certainty to parabolic curvature. Fitting curves to the 18 tracks confirms this with excellent fits over the sample of tracks. See Section VII.

Since there are no noticeable deflections along the tracks indicative of Coulomb scattering, Coulomb scattering is neglected in these momentum estimates.

Momentum was estimated using 18 curved segments in two-tailed tracks using the following criteria:

1. must be a two-tailed track with a vertex
2. one tail must have smooth curvature
3. must have a twin track
4. magnetic field strength is known

The computation below uses the kinetic energy, E_k computed with the general energy loss model in section III A.

For a magnetically charged particle, the analogous formula for parabolic electrostatic deflection for a particle traveling in the x direction in the x, y plane is used

$$y = \frac{e|\mathcal{E}|x^2}{2mv_x^2} \quad (4)$$

substituting B, the magnetic field strength for $\mathcal{E}$, the electric field strength and $g = g_D = (137/2)e$ (Dirac case) or $g = -e$ (Recami-Mignani case), magnetic charge for e, electric charge

$$y = \frac{g|B|x^2}{2mv_x^2} \quad (5)$$

where $mv = p$ and $v/c = \beta = pc/E$ where E is energy, v is velocity and p is momentum. Momentum is given by

$$p_i = \frac{\sqrt{\frac{g|B|x^2}{2y/E}}}{c} \quad (6)$$

where p_i is the ith computed momentum value using known values for x, y and E in (6) Average momentum, $\overline{p}$ is estimated using

$$\overline{p} = \frac{1}{n}\sum_{i=1}^{n} p_i \quad (7)$$

TABLE III. Average momentum values $\overline{p}$, generated from parabolic curvature equation(6) using Recami-Mignani tachyon monopole model for tracks in magnetic fields M1, M2, and M3 as described in Appendix A 2. Energy and momentum values are plotted as E_k vs. p in Fig. 35.

Track	$E(MeV)$	$B(\mu T)$		$\overline{p}(eV/c)$
1.	104.68	M2:	413.52	2.11
2.	93.26	M3:	10,983.73	19.63
3.	496.77	M3:	3290.86	35.07
4.	1314.24	M2:	622.22	22.77
5.	81.12	M2:	10,185.19	20.77
6.	898.04	M2:	396.11	13.20
7.	165.83	M3:	7603.20	15.77
8.	2160.87	M3:	4640.63	61.53
9.	56.30	M2:	779.68	23.93
10.	85.50	M3:	40,740.74	18.31
11.	385.54	M3:	12,369.85	18.65
12.	601.22	M3:	6061.22	28.27
13.	491.24	M3:	6238.19	30.13
14.	682.82	M3:	67,346.94	149.40
15.	153.00	M3:	11,880.00	28.58
16.	199.17	M3:	24,244.90	51.13
17.	106.88	M3:	12,369.85	23.29
18.	116.26	M3:	132,000.00	60.81

V. ζ-CORRECTION

Based on the observation that the particles are traveling in bundles, a correction factor is created

$$\zeta = \frac{w}{w_0} \quad (8)$$

where w_0 is the actual smallest track width measured for a single particle and w is the measured track width of a given track. For this study $w_0 = 5\mu m$. ζ was measured for a number of tracks including the 18 sample tracks. Table IV lists ζ values for selected tracks.

VI. ENERGY-MOMENTUM

The general model for energy loss is used in the following computations.

The measured values of kinetic energy and momentum for our 18 tracks plotted on a graph in Fig. 34 fall in the area for $v > c$ particles. Measured values for kinetic energy, E_k and momentum, p are compared with known particles, i.e. electrons, protons and photons on this graph.
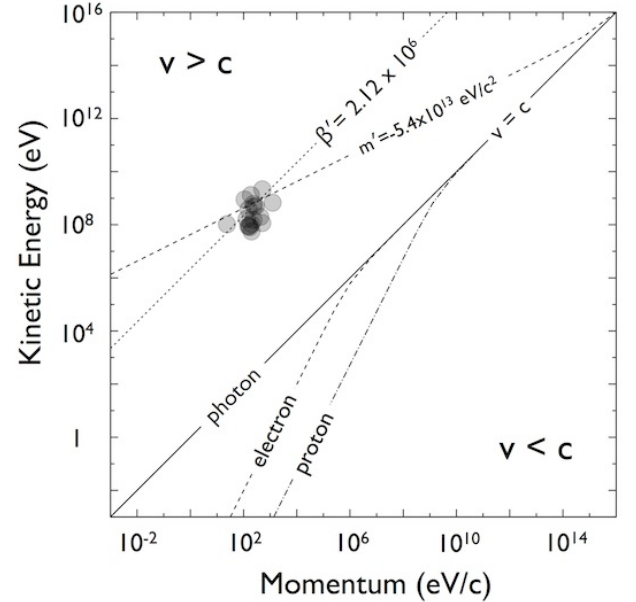
FIG. 34. Measured kinetic energy vs. momentum values for a $g = g_D$ ζ-corrected general model with parabolic curvature. Measured values for momentum and kinetic energy are clustered in the *faster-than-light* ($v > c$) area of the graph with a mass contour line computed with eq. (14) intersecting the peak mass value of $-5.4 \times 10^4 GeV/c^2$. (See Fig. 36). The velocity contour line intersects the average $1/\overline{\beta} = \overline{\beta}'$ value for our 18 tracks using a superluminal transformation of β (see section VIII A). Graph concept after Fraundorf.[38]

FIG. 35. Same as Fig. 34 except monopole charge, $g = -e$ (in Gaussian units), which is a Recami-Mignani tachyon monopole. The difference in charge reduces the momentum value by about a magnitude and pushes the cluster of points further into the $v > c$ region. Peak mass in this case is $-4.5 \times 10^5 GeV/c^2$.
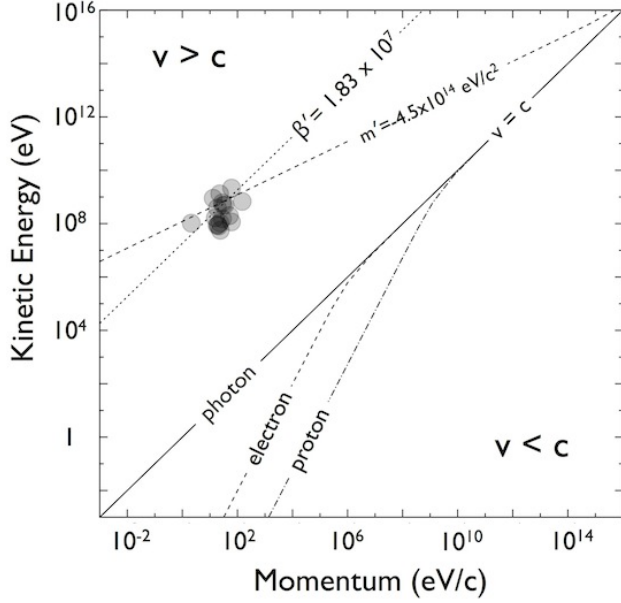
Mass of particle tracks is estimated by inserting measured values of kinetic energy, E_k and momentum, p into the relativistic energy-momentum equation for total energy (assuming $E_k \sim E_{total}$)

$$c^2 p^2 = E_k^2 + 2E_k m c^2 \tag{9}$$

solving for mass,

$$m = \frac{p^2 c^2 - E_k^2}{2E_k c^2} \tag{10}$$

or, in natural units with $c = 1$

$$m = \frac{p^2 - E_k^2}{2E_k} \tag{11}$$

It is found generally that $\beta \ll c$, $m \approx E_k$ and $p \ll m$ and the highest value of γ for our 18 tracks is $1 + 9 \times 10^{-12}$.

To estimate tachyon mass above the $c = 1$ line in Fig. 34, the observables E_k and p need to be transformed from frame f to frame f' using an SLT. In four-momentum notation, $p^\mu = (p_t, p_x, p_y, p_z)$, $E_k \equiv p_t$ and momentum $p = p_x$. To move to frame f' the first two terms of the four-vector are reversed such that $-p'^\mu = (p_x, p_t, p_y, p_z)$. So $E_k' \equiv p_x$ and $p' = p_t$ are substituted into eq. (11) to give

$$m' = -\frac{p'^2 - E_k'^2}{2E_k'} \tag{12}$$

where the values of E and p are interchanged like $E' = p$ and $p' = E$.

Mass contours are found using

$$p = \sqrt{E_k^2 + 2E_k m} \tag{13}$$

for $v < c$ given values of m and E_k and

$$p' = \sqrt{E_k'^2 + 2E_k' m'} \tag{14}$$

for $v > c$, given values of m' and E_k'.

To summarize, average mass and β values using the ζ-corrected general model are shown:

1. Using eq. (11)
   $\overline{m} \simeq -227.58 MeV/c^2 : \overline{\beta} \simeq 1.34 \times 10^{-6}$
2. Using eq. (12) for Dirac tachyon monopoles
   $\overline{m}' \simeq -8.76 \times 10^5 GeV/c^2 : \overline{\beta}' \simeq 2.12 \times 10^6$
3. Using eq. (12) for Recami-Mignani tachyon monopoles
   $\overline{m}' \simeq -7.29 \times 10^6 GeV/c^2 : \overline{\beta}' \simeq 1.83 \times 10^7$

This mass estimate should be taken as a lower limit of particle mass as the assumptions are that $E_k \approx E_{total}$ and that less than the total particle energy is deposited in the track.

The mass and velocity contours for the standard computation using eq. (11) are in the wrong half of the graph (not shown). The lack of agreement between the raw plotted data and mass computed using (11) inclines us to reject the mass and velocity contours and the $|m| = 227.58 MeV/c^2$ value for mass.

Fig. 34 features contour lines for both velocity and mass. While the "raw" E_k and p values are directly plotted on the graph, the contour lines β' and m' on the upper $v > c$ half of the graph were found using a superluminal Lorentz transformation. Since the SLT is a special transformation *only applied in the case of superluminal particles*, this provides a corroboration of the identification of this particle as superluminal.

The estimate of particle mass was made based on a mass contour line intersecting with the cluster of data points. The peak mass values of $|m'| = 5.4 \times 10^4 GeV/c^2$ for Dirac tachyon monopoles and $|m'| = 4.5 \times 10^5 GeV/c^2$ for Recami-Mignani tachyon monopoles from section VI A was inserted into eq. (14) for a range of energy and momentum values and plotted as the dashed mass contour line intersecting the clusters of points respectively in Figs. 34 and 35.

This agreement between the raw plotted E_k and p values, the SLT peak mass, m' computed with (12), and velocity, $\beta' = 1/\beta$ intersecting as contours, constitutes an independent check of the data.

The measured kinetic energy value depends on the estimate of energy loss per grain that was used in the computation. In the general model computation, a 600eV/grain base energy was used with an additional assumption of 150eV/grain for the supplemental pre-exposure energy.

If a base energy of 50eV per grain is used, putting the total energy per grain at 200eV, which is below the minimum value (for 63% of grains to be developed) of 230eV/grain,[35] the minimum kinetic energy value is still well above 10^4eV and still above the $v = c$ contour line.

Measured average momentum depends on eq. (6), the measured kinetic energy and the computed value of the magnetic field. The average momentum values on the plot in Fig. 34 are over two orders of magnitude (eV/c) from the $v = c$ line in the case of the Dirac tachyon monopole and over three orders of magnitude in the case of the Recami-Mignani tachyon monopole.

According to the Recami-Mignani theory, the tachyon should be observed as a monopole in our laboratory frame. Monopoles are not theoretically constrained in terms of mass and under the most basic assumptions, mass is estimated to be either on the order of the unification mass $(\approx 4 \times 10^{15} GeV)$[39] or, based on the assumption that the monopole would have a radius equal to the classical electron radius, $m \approx 2.4 GeV/c^2$. Certain magnetic monopole searches have concentrated in the low to intermediate mass region[40] of $10^3 < m_M < 10^{12} GeV/c^2$. Our lower limit peak mass values of $|m| = 5.4 \times 10^4 GeV/c^2$ and $|m| = 4.5 \times 10^5 GeV/c^2$ are in that range.

The particle is identified as superluminal based on its *measured* values falling in the $v > c$ region of the kinetic energy vs. momentum graphs of Figs. 34 and 35. That the particle is superluminal is corroborated by the need to use an SLT to compute particle mass and velocity. *This operation is required only in the case of a tachyon detected in a bradyonic frame.*

The SLT mass $m' = 4.5 \times 10^5 GeV$ and the SLT $\beta' = 2.12 \times 10^6$ contour lines intersect directly at the measured cluster values.

If a conventional computation is carried out using the energy and momentum data, the resulting mass and velocity contours show absolutely no agreement with the measured cluster of points, intersecting in an unrelated area of the graph.

ζ-corrected energy values are shown in Table IV for *large* tracks and in Table V for the 18 curved tracks.

TABLE IV. ζ-corrected kinetic energy values in the general model for selected tracks.

Track	ζ	$E(GeV)$	$L(cm)$
"loopy segment" 23	50.3	121.0	0.74
"69mm" 11	18.0	402.9	6.90
"67mm"	12.0	262.4	6.74
"bobby pins" 43	4.0	17.3	1.33
"hyper"	7.2	72.4	3.10
"curve swarm" 28	3.0	3.4	0.35
"birds"	2.0	1.6	0.24
"short rev"	6.0	11.8	0.61
"rev caterpillar"	5.0	1.9	0.12
"swarm neg"	3.0	5.5	0.57

TABLE V. ζ-corrected Dirac tachyon monopole (with $g = 68.5e$) using eq. (10) (relativistic) with the general model showing kinetic energy values for 18 example tracks.

number	Track	ζ	$E(MeV)$	$L(cm)$
1.	"classic twins"	2.21	104.68	0.0987
2.	"small hook"	2.59	93.26	0.0122
3.	"hook"	3.47	496.76	0.0914
4.	"bobby pins segment"	4.33	1314.24	0.3290
5.	"hook up"	1.94	81.12	0.0248
6.	"classic 2 tail 1a"	4.17	898.03	0.5336
7.	"classic loop"	1.01	156.83	0.0463
8.	"classic 2 tail 2a"	3.29	2160.87	0.3455
9.	"little mo"	2.82	56.30	0.0339
10.	"a hook"	1.46	86.50	0.0567
11.	"whale 2aa"	3.18	385.54	0.4217
12.	"whale 1a"	2.94	601.22	0.5354
13.	"xray coterm"	5.43	491.24	0.0362
14.	"vector swarm ann."	0.87	682.82	0.0407
15.	"twisting ann."	1.31	153.00	0.1108
16.	"another"	1.68	199.17	0.1925
17.	"2 annihilations"	4.30	106.88	0.1891
18.	"flaming conjunction"	2.39	116.26	0.0569

A. Mass Histogram

A histogram for the distribution of masses, $|m'|$ of the 18 tracks computed using eq. (12) for a tachyon monopole with charge $g = g_D$ and $|g| = |e|$.
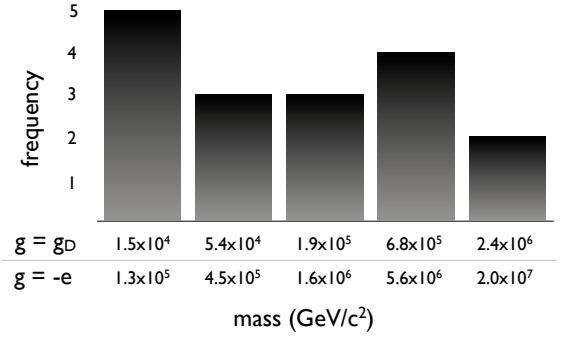

g = g$_D$	1.5×10^4	5.4×10^4	1.9×10^5	6.8×10^5	2.4×10^6
g = -e	1.3×10^5	4.5×10^5	1.6×10^6	5.6×10^6	2.0×10^7

mass (GeV/c^2)

FIG. 36. Histogram of ζ-corrected lower limit mass values for Dirac tachyon monopole ($g = g_D$) and a Recami-Mignani tachyon monopole ($|g| = |e|$) using the SLT eq. (12) in a general energy loss model. The peak value is taken to be $|m| = 5.4 \times 10^4 GeV/c^2$ for $g = g_D$ and $|m| = 4.5 \times 10^5 GeV/c^2$ for $|g| = |e|$.

Our results are compared with the particle energy computed based on Coulomb braking by Urutskoev, *et.al.*.[2] On the basis of the darkening area of a track in the emulsion, kinetic energy was estimated to be $E \sim 700$MeV. This is one order of magnitude different from the average non-ζ-corrected energy value for our 18 tracks of $E \simeq 1.7 GeV$, but on the low end when our long tracks are considered. Other tracks in Urutskoev, *et.al.*[2] and tracks

in the other studies if examined for deposited energy may correspond within our limits. See *e.g.* Table IV. It should also be noted that the energy value is dependent on the model used. In a model (not reported here) where tracks are created by particle radiation mechanisms rather than ionization, the deposited energy is reduced to the level of $\sim 50 MeV$.

Adamenko and Vysotskii[8,9] estimated an upper limit of kinetic energy at $E \sim -10^6 \text{GeV}$ and particle mass at $\approx 10^{-23}\text{g} \ (\approx 560\text{GeV})$.

Our peak mass values presented above fall above the 560GeV value by a couple of orders of magnitude. Our higest non-ζ-corrected energy values come in at $7.3 \times 10^3 GeV$, which falls within the range below the upper limit of $E \sim -10^6\text{GeV}$.

The difference between our numbers and Adamenko and Vysotskii could be due to the bundles of particles effectively masquerading as particles of different mass and energy.

Ivoilov[4] suggests that the particles may correspond to neutrinos, which are monopoles in Lochak's theory[14] and that they may take a maximum value up to the β-decay energy, which in Ivoilov's study was Sr^{90} with electron energy of 2.2MeV and Cs^{137} with electron energy of 0.52MeV.

Our kinetic energy values are generally much greater that this. There does not appear to be agreement between the Ivoilov energy data and ours.

VII. PARABOLIC CURVATURE

In Fig. 37, parabolic curvature can occur for

1. electrically charged particles in an applied *electric* field
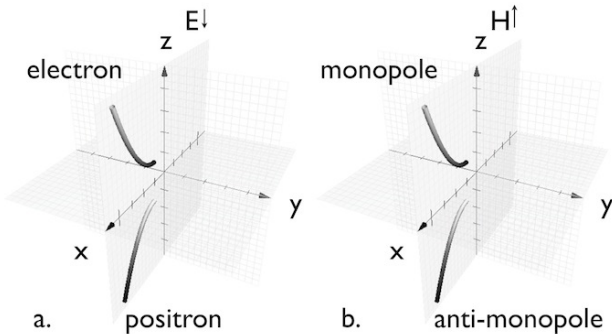2. magnetically charged particles in an applied *magnetic* field

FIG. 37. a.) An electric field, E is applied along the z-axis in the $-z$ direction. Due to the E field, electrons curve upward and positrons curve downward in a parabola in the x, z plane. b.) A magnetic field, **H** is applied along the z-axis in the $+z$ direction. Due to the **H** field, magnetic monopoles curve upward and anti-monopoles curve downward in the x, z plane.

There is no applied electric field in any of our exposures and the curvature is observed in the x, y plane instead of *the x, z plane* where parabolic curvature is expected for a particle with magnetic charge.

The track x, y data for *bobby pins*, the example track, was digitized using the ImageJ package and fit to equation (15), of the generalized quadratic equations

$$y = \frac{\sqrt{-b + (b^2 - 4a(c - x))}}{2/a} \tag{15}$$

$$y = \frac{\sqrt{-b + (b^2 - 4a(c - x))}}{2/a} + o \tag{16}$$

$$y = \frac{\sqrt{-b + (b^2 - 4a(c - x)))}}{2/a}, where$$

$$y = \frac{x}{y} + o \tag{17}$$

which all describe parabolas, where a, b and c are coefficients and o is an offset. The fit target was the lowest sum of absolute square error. Lower numbers for both R-squared and $RMSE$ means a better fit. The mean goodness-of-fit of the generalized quadratic equations to the plotted data is $\overline{R}^2 = 0.998$. Overall, this sample of tracks (and others in the study) show a nearly perfect fit to quadratic equations and therefore to parabolic trajectories.
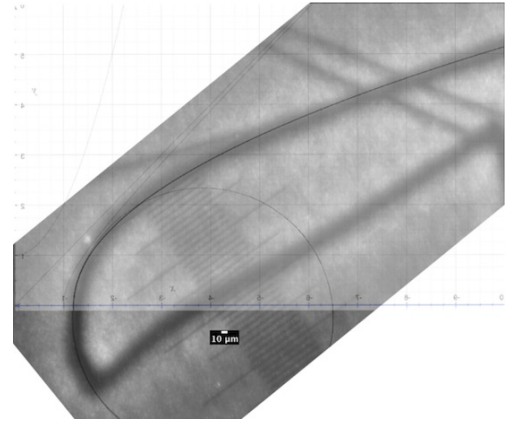

FIG. 38. (1:O) Track 4. *bobby pins* was visually fit in this image to the parabola $y = x^2$ and a circle for comparison.

Parabolic curvature (in the x, z plane) in searches[41,42] for monopoles is considered a strong signature[41,43–45] for a magnetically charged particle since *parabolic curvature is unique.*

But we are seeing parabolic curvature in the x, y plane with a perpendicularly applied magnetic field, so we need to understand what type of a particle could possibly undergo this type of motion.
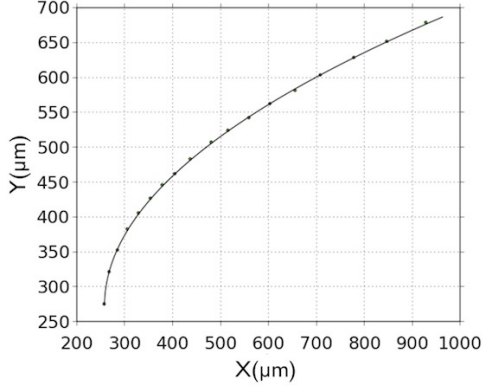
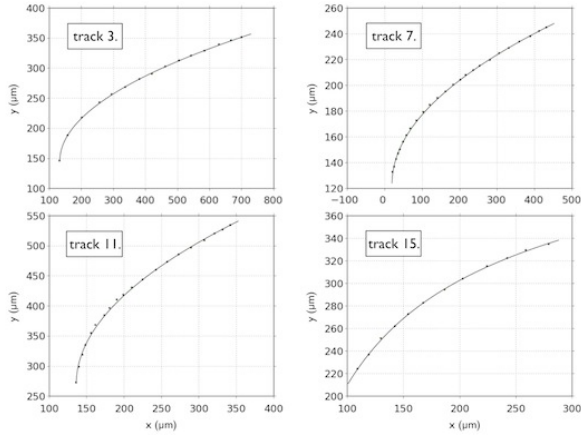FIG. 39. Track 4. *bobby pins* fit to general quadratic eq. (15).

FIG. 40. Tracks 3, 7, 11 and 15 curve fits to general quadratic equations (15), (16) and (17) showing graphical fits to parabolas.

TABLE VI. Goodness of fit (R^2) and root mean square of error (RMSE) for 18 sample tracks fit to quadratic equations.

Track	R^2	RMSE	equation
1.	0.999778	1.2942	17
2.	0.995942	0.3673	16
3.	0.999848	0.7202	16
4.	0.999884	1.2196	15
5.	0.986198	2.1598	17
6.	0.999893	0.7963	16
7.	0.999609	0.6854	16
8.	0.999655	5.1941	16
9.	0.987157	1.1016	17
10.	0.999203	0.6926	16
11.	0.998694	2.8064	15
12.	0.999653	2.1859	16
13.	0.999763	0.9770	15
14.	0.999287	0.6239	16
15.	0.999832	0.7708	16
16.	0.999695	0.6191	16
17.	0.999361	1.7347	16
18.	0.999762	0.3359	16

VIII. TACHYONS

Modern history of tachyons began around the time of Heaviside[46] and Sommerfeld.[47] Though research was temporarily curtailed by ideas about the Tolman paradox,[48] research into faster-than-light particles saw a resurgence in the 1960s with Sudarshan,[49] others,[50,51] and then Feinberg,[52,53] who named the particles tachyons. This was followed by a flurry of theoretical and experimental studies throughout the 1970s and early 1980s seeking, without success, to discover these particles. Today, a number of processes in standard physics, including intermediate states, neutrinos, galactic microquasars, photon tunneling and X-shaped waves are associated with superluminal motion.[54]

Key to the development of the classical theory of tachyons was Recami and coworkers.[55] For a complete description of tachyons, see one of the excellent reviews on the subject.[22,23,55]

Established conventions are used to categorize slower-than-light or subluminal particles as *bradyons*, photons as *luxons* and faster-than-light or superluminal particles as *tachyons*.

A. Superluminal Lorentz Transformation

The transformation from bradyonic inertial frames to tachyonic inertial frames allows us to shift between timelike to spacelike objects. The superluminal Lorentz transformation[20,22,23] (SLT) extends the special theory of relativity to superluminal frames and observers. Most importantly for our purposes, the SLT makes possible the interpretation of experimental data where superluminal and subluminal frames co-exist.

In our experiments, the subluminal frame f can be seen to occupy the same volume element as frame f' but moving with relative velocity $-\infty < |u| < \infty$ with respect to each other. If it is possible to detect a tachyon in a photographic emulsion, then the developed emulsion volume element may be characterized as a snapshot of a slice of a *subluminal volume element* in frame f' where real tachyon observables energy and momentum can be measured. When these real observables are transformed into the superluminal frame f' using an SLT, tachyon properties including mass and velocity can be computed.

A magnetic field applied in the laboratory frame f is simultaneously applied to superluminal frame f', but needs to be transformed according to the rules of the SLT. This means that the magnetic field $\mathbf{H}$ is rotated by either 90° or 270°[22] with respect to the superluminal frame f'.

Parabolic curvature in magnetic fields as shown in section VII is expected of magnetic monopoles, however the curvature is seen (paradoxically) in the x, y plane instead of the x, z plane as expected. The orientation of the magnetic field in our experiments (see Fig. 5) is clearly perpendicular to the x, y plane.

Recami and Mignani[22,23] show the electrically charged tachyon in the bradyonic frame as possessing magnetic charge $g = -e$ (in Gaussian units) as opposed to the "standard" $g = g_D = e(137/2)$. This theory gives a complete symmetry between subluminal and superluminal frames with $v = c$ the partition between frames. Fig. 35 and Fig. 36 show the the data computed with $g = -e$ as in the Recami-Mignani model.

So, in the Recami-Mignani model, superluminal particles in f' with electric charge are expected to behave as magnetic monopoles in our subluminal frame f.
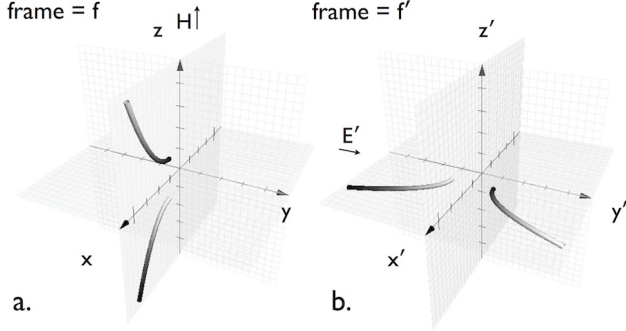

FIG. 41. a. Frame f where a magnetic field applied parallel to the z-axis is expected to cause parabolic curvature for magnetically charged bradyons in the x, z plane. b.) For *tachyons*, parabolic curvature observed in the x, y plane of frame f needs to be interpreted as electrically charged tachyons in the *superimposed* frame f' possessing parabolic curvature in the x', y' plane. For observables connected with electromagnetic fields, frame f' is related to frame f by a superluminal Lorentz transformation where **H** and **E** fields are swapped *and* the coordinate axes are rotated by either $90°$ or $270°$.

By using this transformation we rectify the paradox of parabolic particle tracks observed in the plane perpendicular to the applied magnetic field where we expected circular tracks. This is due to the transformation of the **E** and **H** fields[22,23] (**B** can be converted to **H**)[56] where moving between frames, the axes are swapped so that $\mathbf{H} \rightleftarrows \mathbf{E}$.

Thus it is possible to interpret our parabolic tracks in photographic emulsions as due to electrically charged tachyons sampled with a bradyonic slice of a tachyonic volume element transformed using an SLT. The electrically charged tachyons behave like magnetically charged bradyons, that is like magnetic monopoles in our slower-than-light frame, with the exception that *the plane of parabolic motion in magnetic fields is rotated by* $90°$ *or* $270°$.[22]

Measurement of the parabolic curvature of these tracks also importantly allows us to estimate the particle momentum using eq. (6).

The E_k vs. p graphs in Figs. 34 and 35 presented in section VI show clusters of data points in the $v > c$ region.

If a tachyon has been detected in the laboratory frame, then the observables, E_k and p need to be transformed from the bradyonic frame f to the superluminal frame f' to find mass as was done with the energy momentum equation, eq. (12) in section VI. As shown above, the SLT results in the values of E_k and p being interchanged such that $E' = p$ and $p' = E$. Velocity of the tachyon is found with $\beta' = 1/\beta$.

As mentioned earlier, the requirement of the SLT to obtain the correct mass and velocity of the particle provides confirmation of the particle identification as a tachyon.

ζ-corrected values for a superluminal Dirac monopole using a general energy loss model with charge $g = 68.5$ and parabolic curvature are shown in Table VII.

TABLE VII. Momentum p, mass m', and β' for 18 sample tracks based on a ζ-corrected Dirac tachyon monopole with $g = 68.5$ Mass is calculated using eq. (12). $\beta' = 1/\beta$.

Track	$p(eV/c)$	$m'(eV/c^2)$	β'	$B(\mu T)$	
1.	23.77	2.3×10^{14}	4.4×10^6	M2:	413
2.	162.46	2.7×10^{13}	5.7×10^5	M3:	10,983
3.	290.28	4.2×10^{14}	1.7×10^6	M3:	3290
4.	188.46	4.6×10^{15}	7.0×10^6	M2:	622
5.	171.91	1.9×10^{13}	4.7×10^5	M3:	10,185
6.	109.28	3.7×10^{15}	8.2×10^6	M2:	396
7.	130.49	1.1×10^{14}	1.3×10^6	M3:	7603
8.	509.28	4.6×10^{15}	4.2×10^6	M3:	4640
9.	198.03	8.0×10^{12}	2.8×10^5	M2:	779
10.	151.51	2.5×10^{13}	5.7×10^5	M3:	40,740
11.	154.38	4.8×10^{14}	2.5×10^6	M3:	12,369
12.	233.98	7.7×10^{14}	2.6×10^6	M3:	6061
13.	249.35	4.8×10^{14}	2.0×10^6	M3:	6238
14.	1236.49	1.9×10^{14}	5.5×10^5	M3:	67,346
15.	236.55	4.9×10^{13}	6.5×10^5	M3:	11,880
16.	423.16	4.7×10^{13}	4.7×10^5	M3:	24,244
17.	192.74	3.0×10^{13}	5.5×10^5	M3:	12,369
18.	503.29	1.3×10^{13}	2.3×10^5	M3:	132,000

IX. DISCUSSION

The particle tracks in our studies occur independently of dielectric isolators and thus are not due to chemical effects from human fingers. Some exposures in our studies show tracks where there is no contact of fingers. Observations in several other studies[2,4,7,10,11] show sets of tracks with virtually identical structure in completely distinct experimental setups with no contact of fingertips.

The patterns shown in the majority of studies suggest tracks due to particles in regular periodic motion and possibly helical motion. Observation of magnetic field effects on groups of correlated particles causing individual particle deflections is conclusive evidence for the recording of particles in fields.

The nature and the scope of the data indicates a new particle, not previously categorized, possessing a number of specific properties.

A. Curvature

For a particle with electromagnetic charge, curvature of tracks can be the result of the earth's magnetic field, an applied magnetic field, an applied electric field or combinations thereof.

The tracks observed in our experiments where a magnetic field was applied perpendicular to the plane of the photographic detector ($[x, y$ plane in frame $f] \rightarrow [x', y'$ plane in frame $f']$ of Fig. 41) are parabolic. In a perpendicular applied magnetic field (*i.e.* parallel to to the $+z$ direction in frame f of Fig. 41), the only particle expected to have a parabolic trajectory is a magnetic monopole. But, it is expected to exhibit curvature in the x, z plane instead of the x, y plane. This was resolved using the Recami-Mignani classical theory of tachyons where faster-than-light particles exhibit symmetry with ordinary slower-than-light particles. Particle energy, momentum, velocity, mass and electromagnetic fields are transformed between subluminal and superluminal frames using an SLT.

An electrically charged tachyon in a superluminal frame is transformed into a magnetically charged bradyon in a subluminal frame. Observation of parabolic curvature in the x, y plane with a perpendicular applied magnetic field implies the detection of tachyons in a subluminal frame.

Application of parallel electric fields may produce circular curvature for these particles. Application of pulsed electric or magnetic fields may make possible time-of-flight measurements for these particles.

B. Random Motion

Random motion of these particles is one of the most interesting properties observed. What mechanism can cause the particle to abruptly change direction while, in the case of correlated random motion, maintaining lock step with its partner (or partners)?

1. Collision - A particle moving in a straight line collides with the randomly distributed components of a photographic emulsion creating a random trajectory. This case apparently fails because it is dependent on the random structure of the medium and, as such, will not result in correlated trajectories.

2. Radiation - In the analysis of the Čerenkov radiation of tachyons it is possible for the particle to emit individual quanta at any energy up to the total energy of the tachyon. Large-angle deflections in these tracks may correspond with the idea of the successive random emission of quanta in a radiating particle where the emitted particle momentum is large with respect to the tachyon momentum. Analyses of the various regimes of motion of tachyons, show that random motion trajectories may be expected.[57,58] (See Fig. 42). At random

intervals, the tachyon gives up a quantum with a loss of a random quantity of energy resulting in a recoil angle from $0°$ to $180°$. The highest energy quanta result in the emission directly in front of the tachyon and create a recoil with a very large angle deflection.

This case depends on the internal state of the particle and so if this state is shared with other particles with which it is entangled, this process may be considered as a candidate for random motion of this particle. The velocities calculated in Section VI and VIII A from measurements however argue against a mechanism of Čerenkov radiation (or radiation at all) due to the high velocities of the tachyon.

3. Intersection with Light Cone - A tachyon can go into a state of chaotic motion at certain speeds due to a radiative reaction force. In this approach,[59] the tachyon's helical trajectory itself may contribute to its chaotic motion by intersections with its own light cone. See *e.g.* Fig. 1 of [59].

This mechanism also depends upon the particle's internal state and like the radiation mechanism in case 2 could lead to correlation if the radiative reaction force state is shared between entangled particles.

Thicker emulsions should be able to reveal additional details regarding the random motion trajectories, particularly if they are being constrained by internal reflection of the emulsion/air and emulsion/base interfaces.
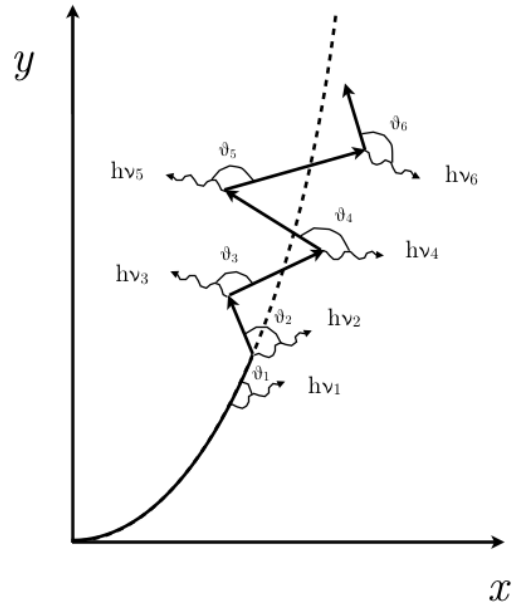

FIG. 42. Random motion trajectory schematic (after Fayngold[60])

C. Correlation

The particles possess a property of correlation. Strongly correlated particles are often observed in conjunction with applied magnetic fields and either smooth regular curved or random motion tracks.

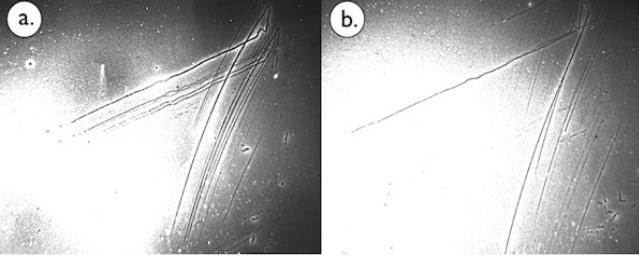Correlation of particles is simply explained using the allowed $T \to T + T$ decay mechanism.[52]

FIG. 43. (1:O) *bobby pins* raw tracks in Kodak NTB3 10μ emulsion. Tracks a and b are separated by a few millimeters on the film. Tracks have many of the same features, except that track a has a loop, *i.e.* the track crosses itself whereas track b does not. These tracks are correlated in position extremely well until the critical region (segment 19 in Fig. 44.) when track a has a large angle deflection to the left and track b has a corresponding smoothly curving deflection to the right. Susceptibility to magnetic deflection appears to be overwhelming or twisting the correlation.
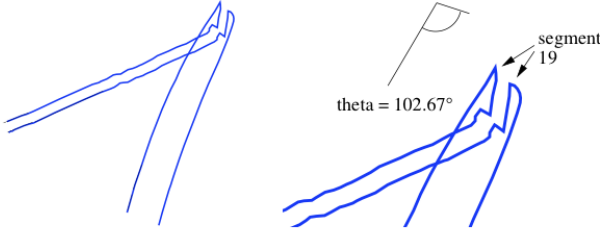

FIG. 44. Digitized tracks from Fig. 43

Measurements of position and momentum for the swarms we have shown here would be correlated in both position and momentum. A perfectly correlated EPR pair of particles obey $\Delta(p_1 + p_2) = 0$ and $\Delta(x_1 - x_2) = 0$, but since they are not perfect, we can use[61]

$$\Delta(p_1 + p_2) < min(\Delta p_1, \Delta p_2),$$
$$\Delta(x_1 - x_2) < min(\Delta x_1, \Delta x_2) \tag{18}$$

Faster-than-light communication is, of course, at the center of the entire ongoing debate regarding the EPR paradox, Bell's Theorem, and measurement in quantum theory. Tachyons can be considered to be a potential mechanism of the correlation itself[62] and, as such, a fundamental building block of the universe. Fayngold[63] recently proposed tachyons as the mechanism for superposition, which relates directly to measurement and entanglement.
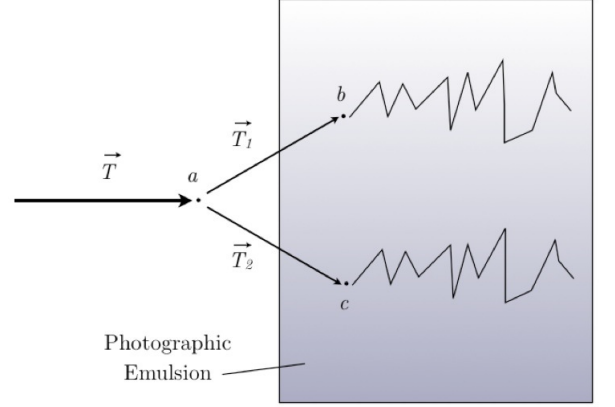

FIG. 45. How the $T \to T + T$ transition may produce correlated random motion trajectories on a photographic detector. At point a the particle decays into 2 or more particles. At points b and c, the now lower energy particles enter the photographic detector and may go into random motion. Decaying particles like this may be naturally entangled. Because of entanglement, each particle would be observed in the detector to be correlated.

In Soucek's subquantum model,[64] which features faster-than-light particles, correlated random motion, shown here in Section II K, is a testable feature of the theory. Tachyons also can fit well as the missing piece in hidden variable theories. See discussion in [65].

There are relativistic explanations of dual images for tachyons, *e.g.* the *double images* of Tomaschitz[66] or the *optic boom* of Barut, Maccarrone and Recami[67] but it is not clear how this would apply in the case of particles going through an emulsion. In other words, we are not just taking a picture of a tachyon, the physical particle is traversing the emulsion.

Lochak[14] sees correlated tracks in the study of Iviolov[4] as chrial tracks. Lochak presents an interesting discussion on how these tracks may be created on double-sided X-ray film using glass or a monocrystalline Ge or Si reflector. Lochak and Ivoilov also mention that the two chiral tracks have a geometric center (with a rotation between the tracks of π). This observation appears to be related to the geometric center we have observed in images such as Fig. 29. There are other *normally correlated* tracks appearing on the same image (see Ivoilov in B) although they are too faint to be analyzed in detail in the reproduction.

Based on the observations of bundles, the most straightforward explanation of correlation appears to be splitting of bundles of entangled particles which share state (*i.e.* momentum) leading to correlated movements due to a random energy loss process.

Correlation is a central feature of this particle.

D. Regular Periodic Motion

Regular periodic structure has been observed for very wide tracks as well as the thinnest tracks. The periodic structure suggests a particle moving with a very tight helical motion or some type of regular periodic/chaotic motion around the track center. Patterned tracks such as the "beaded necklace" or "caterpillars" may suggest some type of *poinsot*[14] or *chaotic* top mechanism.

If tachyonic, this may be similar to the helical motion analyzed by Davidson[59] or Ibison,[68] which defines chaotic modes at the intersection of the helix and the light cone.

The Dirac equation for tachyons features specific helicities for tachyons and antitachyons.[69] For the sizes of the helixes observed and the resolution of photographic emulsions, given enough data, it should be possible to distinguish visually between right-handed (antitachyon) and left-handed (tachyon) helixes if they exist.

Recami[23] has suggested a *vacuum fluctuation* propagating in space as a series of tachyon creations and annihilations on a world line that looks like a zig-zag track (see Fig. 16 and Fig. 35 of [23]).

The highest magnification images of evaporated tracks indicate a mechanism corresponding more to a vacuum fluctuation type track comprised of a collective excitation rather than the helical type track. Thicker emulsions may assist here to evaluate the real structure in three dimensions.

One of the biggest questions to be answered will be what mechanism causes the periodic tracks and if it is a spin-like motion, a collective excitation type effect or something else.

E. Bundles

The track structure analysis and track width measurements in this study and in the studies of Urutskoev and Ivoilov bring up some interesting questions as to how a single particle can have track widths in our case from $\sim 5\mu m$ to $110\mu m$ and in their case $5\mu m$ to $30\mu m$. In the Russian studies they note that upon moving the detection apparatus away from the reaction vessel by more than a meter, the track width decreases. According to Lochak and Urutskoev:[18]

> We have experimentally found that the larger is the distance between the detector and the unit center, the narrower is the trace pattern. At a distance equal to about half a meter the width is about $30\mu m$, while at a 2-meter distance it is only around $5\mu m$.

In our measurements, tracks corresponding to the high energy regime, that is, straight or smoothly curving tracks, are measured to be $40\mu m$ to $110\mu m$ tracks corresponding to a lower energy regime such as random motion, correlated twins or correlated swarms are measured to be $5\mu m$ to $20\mu m$.

In Section II L, images of tracks show internal structure and splitting or unraveling of tracks possibly indicating that these particles travel together in bundles.
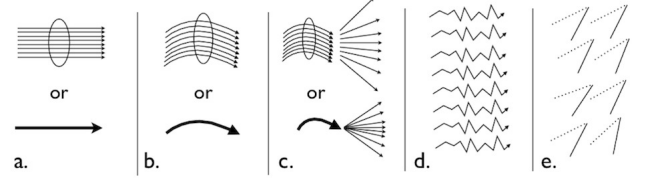

FIG. 46. Energy transition of tachyon bundle or single tachyon in a photographic emulsion in an applied magnetic field. a.) bundle or single tachyon at highest energy is seen as nearly straight single track. b.) bundle or single tachyon energy becomes susceptible to magnetic field exhibiting smooth curvature. c.) bundle decreases in energy further and individual strands become susceptible to magnetic field causing bundle to unravel or single tachyon splits into multiple low-energy particles. d.) low-energy tachyons now are measured in the photographic emulsion and exhibit entanglement in position and momentum. Low-energy tachyons lose energy now via emitted quanta with momenta that is large with respect to the tachyon momentum, causing random motion due to recoil of emitted quanta. e.) the tachyon energy goes to zero and it undergoes annihilation with its antitachyon.

One can view dual and multiple correlated tracks in photographic emulsions as a real correlation of tachyon particle tracks due to the $T_{bundle} \rightarrow T + T$ or $T_{bundle} \rightarrow T_{bundle} + T_{bundle}$ decay where a single tachyon or a multiplexed tachyon bundle decays into one or more entangled lower energy correlated pairs and swarms of tachyons.

Schwartz[70] has recently shown an analysis of tachyons traveling in bundles due to gravitational attaction within the general theory of relativity. This is the only mention of tachyons traveling in bundles known at present. Further study is needed to understand any connections with our observations of bundles in Section VI and splitting of bundles in magnetic fields Section II L.

Since these particles appear to travel in bundles, we defined a factor $\zeta = w/w_0$ in Section VI) where w_0 is the actual smallest track width for a single particle and w is the measured track width of a given track. Particles traveling in bundles might be visualized as *beams* rather than single particles.

F. Creation and Annihilation

Feinberg,[52] and others have shown that tachyons may be both created and annihilated in pairs.

In correlated groups of tracks and generally in our data and in the other studies, we often see long track tails that co-terminate (co-initiate) or undergo a large-angle deflection at vertexes, the angle of which has been measured to be between $8°$ - $110°$. Also in the tails leading up to vertexes, there are often increasing large angle deflec-

tions. Vertexes of particular interest are comprised of one straight track and one parabolic track.

In differential deflection analyses of correlated particles, (which is the subject of ongoing work), we measure momentum decreasing in correlated tracks culminating in minimum momentum at co-termination points. (See *e.g.* Fig. 43). It is possible that singularities at these vertexes are tachyon-antitachyon annihilation (creation) events (and/or tachyon tunneling at classical turning points). A proposed two-tailed tachyon-antitachyon annihilation signature is two co-terminating (co-initiating) tracks, where, just prior to (after) the termination (initiation) point, one track exhibits smooth curvature to (from) the termination (initiation) point.

G.   Correspondence with Other Studies

There is a specific correspondence of a subset of this data to certain data and analysis shown in the studies of Urutskoev, *et.al.*.[2], Ivoilov.[4], Rodionov and Savvatimova[10], Priem, *et.al.*[6] and Bardout, *et.al.*[7] and Adamenko and Vysotskii[8] The analysis and interpretation of these results by Lochak in [14],[18], and [7] and also the analysis by Adamenko in [8] and [9] as monopoles harmonizes with our observations and even the possible interpretation of these particles as tachyons due to the correspondence between monopoles and tachyons.[19,22,23,67,71]

In the other studies, we see regular periodic tracks, large angle deflections, a range of sizes of vertically incident tracks (dots), and correlated trajectories (mentioned mostly as *parallel* trajectories). But, other studies do not mention observations of correlated random motion tracks or correlated groups of tracks. Only Priem, *et.al.*[6] mentions tracks with smooth curvature in *electric* fields and random motion tracks and Bardout, *et.al.*[7] mentions curvature in the earth's magnetic field.

The other studies have yielded a collection of data quite similar to our experiments where we used no pre-exposure amplification and constant agitation during development. Our studies have generated a much larger set of data comprised of effects we associate with lower-energy ranges of the particles such as random motion. *Photographic amplification used in our studies appears to have clearly extended the range of detectable particle effects.*

It would be of great interest to use our amplified emulsions in the other types of experiments where these tracks have been observed.

H.   Interesting Factors

Positive tracks can be created via either a particle radiation or non-radiative mechanism. The photon or electron interactions of a particle interact with our pre-exposed AgBr grains and create a track in the image of the particle at a density level above the pre-exposed background density level. Reversed tracks on the other hand, create a condition to teardown latent images created by the pre-exposure by somehow making the Br^0 ions recombine with the Ag^0 latent image. There are a few mechanisms available to do this having to do with a different, higher level of exposure of light, but these may not make sense for a particle traversing the emulsion.

Observation of *evaporated* tracks indicate a direct action of the particle to *melt* surfaces that may or may not be accompanied by exposure of the AgBr grains. This mechanism is of great interest in light of studies showing corresponding tracks on palladium electrodes[10] and on metal dielectric semiconductor surfaces[8].

Once injected into the AgBr/Gelatin region between the film base and the gelatin/air interface, the particles seem to travel for very long distances in the film, which, as we have mentioned before, is not microscopically flat in these experiments. Ivoilov[4] has put forth the idea that particles can be captured at a low angle of incidence and become "trapped" by a mechanism of internal reflection between the base/gelatin and gelatin/air surfaces. This type of mechanism is required to explain how long tracks of up to 69mm in length and the random motion tracks are recorded.

This hypothesis can be tested with emulsions of varying thickness and microscopic analysis of tracks to see if trajectories are reflected at the gelatin/air and base/gelatin interfaces.

The probability of capturing events such as magnetic curvature and random motion in two dimensions is a function of particle number density. Track number density has been found to be as high as 100 per square cm during the exposure period. Particle number density can be determined using the experimental methods shown here.

Correlated swarm behavior in magnetic fields is of great interest, particularly where there are differences between individual elements of the swarm. Also of interest are "two tailed" correlated tracks with one or more large angle deflection between the tails. Differences between correlated trajectories in magnetic fields may indicate monotonic changes in energy and momentum, indicating particle direction and possibly points of creation or annihilation.

Positive and reversed correlated random motion tracks and smooth curvature tracks have been observed both as periodic structure tracks and smooth saturated tracks. Splitting has been observed for both positive and reversed tracks. But, periodic structure has not been observed where bundles appear to be splitting. One possibility is that bundles and higher energy tracks show up as saturated, but lower energy tracks can transition from saturated to more sparse periodic structure tracks. This may be what is happening in Fig. 29 in the minimum energy points of the track where we see saturated track segments transitioning to periodic tracks. This will be an area of interest in the future.

More detailed study of these particles is envisioned to generate new data using emulsions of varying thickness with calibrated amplifying pre-exposures using a sensitometer in calibrated magnetic fields along with higher resolution microscopic analysis of tracks.

It may be possible to differentiate particles of opposite helicity or charge, that is particles and antiparticles, using photographic analysis.

X. CONCLUSION

A. How could we have missed these particles?

Even though photographic emulsions have been around since the 1700s and have been the subject of intense scientific research, it is possible that *these particle tracks are essentially a very weak effect* with respect to the standard sensitivities of photographic emulsions that was in some cases simply not seen, in other cases overlooked, and in yet other cases *recognized* as a type of *known defect.*

Lochak[14] speaking of the experimental work of Ivoilov mentioned that some data might have simply been discarded, having identified it as surface defects or scratches.

> ...Ivoilov noted on the photographic plates myriads of *microscopic tracks* [emphasis added] that did not draw attention at first glance, as they looked as small defects of the surface. On closer inspection, however, it turned out that the microscopic tracks were not simple defects.

In our own work, we did not recognize particle tracks until we used pre-exposed emulsions and did not agitate in photographic development, which greatly increased the signal-to-noise ratio. An entire series of earlier experiments that did not show any track data, later, under microscopic examination, revealed numerous tracks.

It is possible that this is an ambient background effect and we should examine photographic films in general for these effects. Our study indicates that photographic detectors at higher levels of amplification are sensitive to additional particle track effects not picked up by those at standard levels of sensitivity.

B. What is the source of the particles?

Comparing our work, where particle tracks were seen without electrical discharge devices, with other experiments where a diverse array of discharge devices was used, raises a question about the source of the particles. In fact, a much wider array of particle track behavior is seen in our experiments.

On one hand the evidence appears to indicate that tracks occur due to electrical discharges, explosions, excitation of beta-decay products or glow discharges and their by-products. On the other hand, a complete assortment of the track types has been observed without any discharge or reaction whatsoever. A possible explanation is that the particles exist as a natural background and their appearance is being amplified by these experiments.

Adamenko and Vysotskii[8] call out the issue stating the effect is either due to the very strong squeezed magnetic field in the collapse zone of their electrical discharge apparatus or *external to their laboratory* in the very strong squeezed cosmological magnetic fields.

Ivoilov[4] defines a *control background* and observed this background to vary in time and to be correlated with the quantity of tracks due to the arc discharge and considers the possibility that this background is cosmic radiation.

Future experiments are indicated to distinguish between a local source and an ambient background of particles.

C. Summary

The evidence here suggests the detection of Dirac tachyon monopoles with a lower limit of $|m| \sim 5.4 \times 10^4 GeV/c^2$ or Recami-Mignani tachyon monopoles with a lower limit of $|m| \sim 4.5 \times 10^5 GeV/c^2$ that can travel in bundles of "identical" particles with periodic or possibly helical trajectories with different modes, dependent on energy level. At lower energies, the particle may go into random motion. Correlation of pairs and groups of these particles is observed frequently.

In Section VI graphical analysis shows measured energy and momentum for our sample tracks in the $v > c$ sector of the graph, indicating superluminal particles. The $v > c$ result is supported by the requirement to transform the data using an SLT to yield consistent mass and velocity values.

In Section VII parabolic curvature is observed in an applied magnetic field as would be expected for a magnetic monopole, except that the parabolic curvature is in the x,y rather than the x,z plane. Parabolic curvature in the x,y plane *perpendicular* to an applied magnetic field suggests the detection of a magnetic monopole in our local frame, which as shown in Section VIII A is how an electrically charged tachyon in a coincident superluminal frame would appear in the local frame.

The Recami-Mignani classical theory of tachyons[22] gives a solid framework for the study of these particles based on an extension to the special theory of relativity where electrically charged tachyons can also be magnetic monopoles. The superluminal Lorentz transformation as expounded by Recami and Mignani has supported both the correct results for mass and velocity as well as the concept of parabolic curvature of tachyons in a transverse magnetic field.

Four pieces of evidence support the identification of these particles as tachyons:

1. E_k vs. p plot shows a cluster of data points in $v > c$ region

2. Given energy and momentum observables in the laboratory frame, an SLT is required to compute mass and velocity of tachyon
3. Parabolic curvature is a unique signature for monopoles
4. An SLT applied to the plane of parabolic curvature indicates tachyon monopoles

Further study of the image formation, energy deposition, curvature in magnetic fields, bundling, splitting, vertexes and correlation of these particles is indicated to get a clear picture of their properties.

Appendix A: Photographic Techniques

1. First Series: 1977

Contact exposures of fingertips without amplification were done in a darkroom in total darkness or with Kodak type 1A safelight.

Polydisperse and Lith (monodisperse) type emulsions were used with exposure times of 2 minutes with no pre-exposure, and standard processing using constant agitation. The film was placed on a thin plastic sheet affixed to a 6 x 3 inch copper board. The finger tips were placed directly on the emulsion side of the film for an exposure time of 120 seconds. The film, after exposure, was processed and dried.

Lith film, either Polychrome or Kodak Kodalith type III, was processed using constant agitation in Kodak Kodalith developer at standard dilution for 2.5 minutes.

TABLE VIII. Constant agitation processing for litho films. All temperatures at $20°$C.

step	solution	time
Kodak Kodalith Ortho type III or Polychrome Litho Film		
1. Dev.	Kodak Kodalith Super RT[a]	2.5 min
2. Stop	water	10 sec
3. Fix	Kodak Fixer	5 min
4. Wash	running water	20-30 min
5. Dry	dust-free atmosphere	30-60 min

[a] Low-sulfite hydroquinone developer, primarily surface image development. Constant agitation in development.

Kodak Plus-X film was processed using normal agitation in D-76 developer at standard dilution for 2.5 minutes.

Kodak Ektachrome film used a standard E-6 processing program provided by a third party processor.

2. Second Series: 1979, 2001

Contact exposures of fingertips with amplification were done in a darkroom in total darkness.

TABLE IX. Processing for Plus-x film. All temperatures at $20°$C.

step	solution	time
Kodak Plus-X type Film		
1. Dev.	Kodak D-76 developer (full strength)[a]	5.5 min
2. Stop	water	10 sec
3. Fix	Kodak Fixer	5 min
4. Wash	running water	20-30 min
5. Dry	dust-free atmosphere	30-60 min

[a] metol-based solution physical developer, surface and internal image development. Normal agitation in development.

Three types of permanent magnets were used to apply magnetic fields in the exposure region of the photographic emulsion:

1. M1 - AlNiCo cylindrical diametrically magnetized magnet producing $\sim 50G$
2. M2 - NdFeB cylindrical magnet producing surface field of $2681G$, $Br_{max} = 13,200G$, $BH_{max} = 42MGOe$
3. M3 - NdFeB block producing surface field $3411G$ $Br_{max} = 14,800G$, $BH_max = 52MGOe$

In the case of $M2$ and $M3$ the value of B for each track is found by applying the inverse square law to the measured distance from the track to the known value of the magnetic field of the permanent magnets based on a diagram provided by the manufacturer.

Kodak Kodalith Type III or $10\mu m$ Kodak NTB3 nuclear track emulsion on a polyester base was prepared with a non-standardized uniform pre-exposure[72] consisting of a brief 1/2 to 1 sec. exposure to diffuse tungsten light which resulted in approximately 0.6 - 4.0 density units on the processed film.

The fingers of the hand were placed on the emulsion surface for an exposure time between 5 and 30 minutes, and no agitation was used in the development phase of lith development using Kodalith developer at standard dilution.

Agitation in the development stage of emulsion processing, commonly used to prevent the build-up or uneven flow of development by-product,[30] also produces image spread. The less image spread that is produced, the greater the accuracy of measurements performed on track images. Especially for very thick emulsions, agitation may cause distortions and is not desirable in the development of emulsions for nuclear track studies.[73]

TABLE X. Processing for monodisperse emulsions. All temperatures at 20°C.

	Kodak NTB3 Nuclear Emulsion or Kodak Kodalith Ortho type III	
step	solution	time
1. Dev.	Kodak Kodalith Super RT (1:1)[a]	2.5 min
2. Stop	water	10 sec
3. Fix	Kodak Fixer	5 min
4. Wash	running water	20-30 min
5. Dry	dust-free atmosphere	30-60 min

[a] Low-sulfite hydroquinone developer, primarily surface image development. No agitation in development.

Appendix B: Comparison with Other Studies

Here comparisons are shown between the Fredericks data shown in this paper and the studies of Urutskoev, *et.al.*[2], Iviolev[4], Bardout, *et.al.*[7], Rodionov and Savvatimova[10], Priem, *et.al.*[6] and Adamenko and Vysotskii.[8]

It is difficult to show an accurate cross section of all of the tracks with over 200 exposures and thousands of tracks. There are many other matching images between Fredericks and other studies that could be shown. However the correspondence between Fredericks and other studies is clearly shown. Common properties can also be seen between the other studies.

As mentioned earlier, the only track property specifically not contained within our datasets is the Ivoilov "chiral" type track. This is most likely due to the requirement of double-sided X-ray film and a metal mirror substrate in these exposures, which we did not have in our experimental setup.

In the cases of the other studies, we took the track images from the original papers and the images are often low-resolution and not reproduced in the best possible manner. In many cases we have used image processing techniques in order to see the tracks more easily.

1. Urutskoev, *et.al.*

Urutskoev, *et.al.*[2] described experiments using film types RF-ZMP, a fluorographic film at 0.85 (density units) above haze, a radiographic medical film RM-1MD at 0.85 (density units) above haze, and nuclear photo plates "type R" with 100 μm thickness. D-19 developer for 6 min. at 20° C was used for the fluorographic films and an isothermal method of development was used for the nuclear plates in a phenidone-hydroquinone developer.
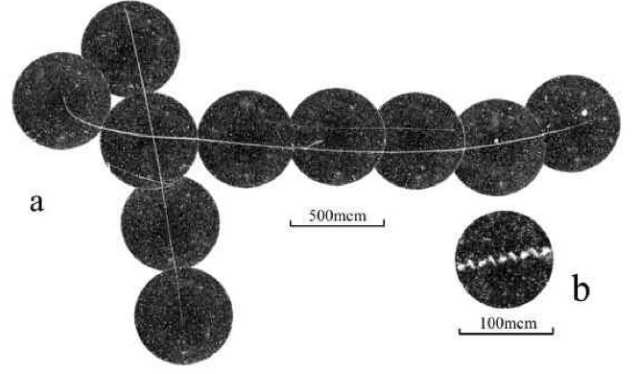
FIG. 47. a.) Entire tracks in fluorographic film RF-ZMP with emulsion layer thickness $10\mu m$. b. Closeup of section of track showing periodic structure.)
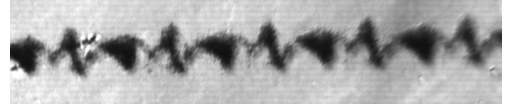

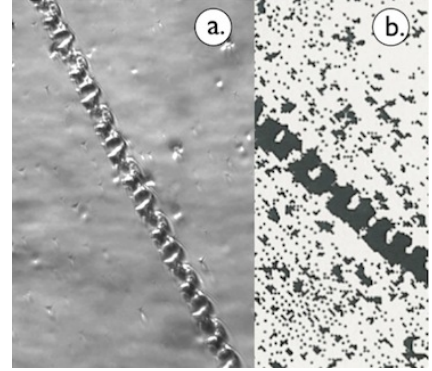FIG. 48. Magnified section of Fredericks track matching Fig.47b.

FIG. 49. a.) (3:O) Fredericks caterpillar track. Kodak Kodalith type III film. b.) Urutskoev caterpillar track.
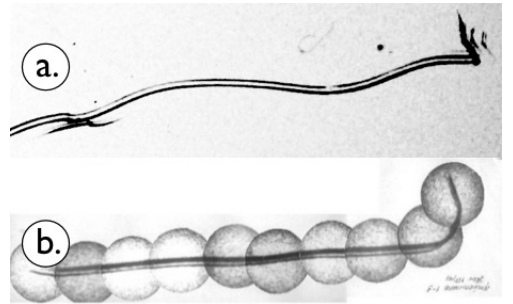

FIG. 50. a.) (1:O) Fredericks track in Polychrome Litho film. Compare with tracks in Section II L *Track Bundles* and Fig. 6 in Priem, *et.al.* [6] b.) Urutskoev track. "Typical track" of Urutskoev and co-workers.
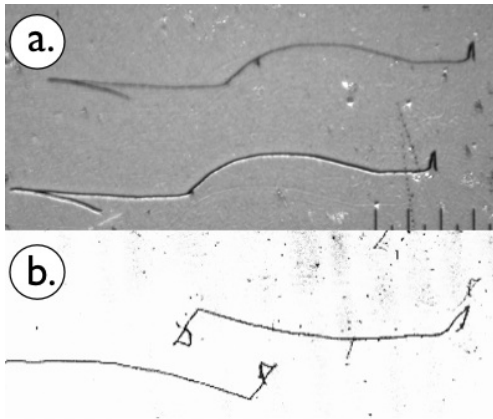
2. Ivoilov

FIG. 51. a.) (1:O) Fredericks tracks. Correlated tracks in Kodak Kodalith type III film. Tracks are copies instead of mirror images or chirally transformed. b.) Iviolov "chiral" tracks. Multiple correlated tracks can be seen in the original image. The chirally transformed track is explained in the Ivoilov analysis as a reflected track which is recorded on the bottom emulsion facing an aluminum plate with polyester base material sandwiched between the 2 emulsion layers. Unspecified type of double-sided X-ray emulsion.

The most interesting thing about Fig. 51 is the long tail track structure leading up to large-angle deflections and the main vertex(es) in the center of the image. These are entirely reminiscent of Fig. 29.
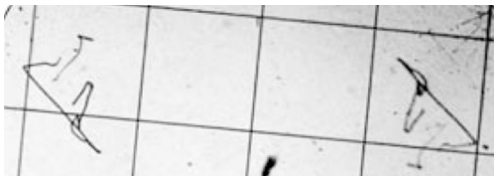
FIG. 52. Ivoilov "chiral" tracks in original orientation

FIG. 53. Ivoilov "chiral" tracks where right track was flipped horizonally and vertically and overlaid on left track. Note correspondence on main track and misalignment on other tracks. Compare with Fredericks tracks in Fig. 27 where 2 correlated tracks are overlaid

.
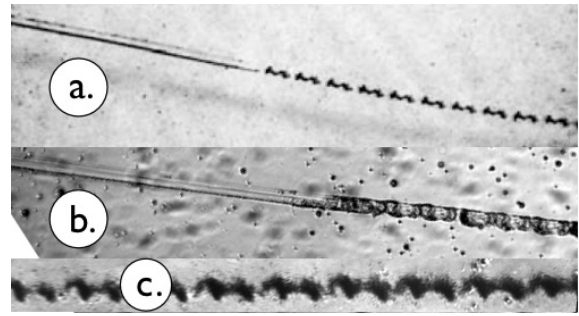
FIG. 54. a.) Ivoilov track changing from smooth to periodic structure. b.) (3:O) Fredericks track changing from smooth to periodic structure. c.) (1:O)Fredericks track showing similar structure to periodic portion of a.

3. Bardout, *et.al.*

An image from Bardout, *et.al.*[7] exposed on an expedition to the north pole using the double-sided X-ray film, Kodak Industrex MX125, is compared with a Fredericks image in the present study generated with magnet M3 on Kodak Kodalith type III film.
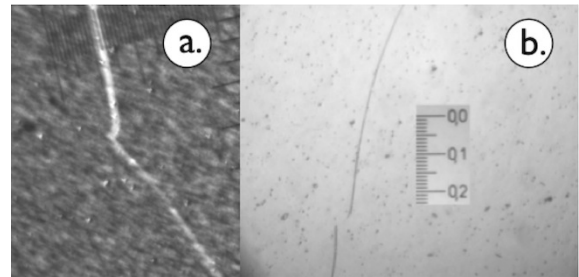

FIG. 55. Both of these are classic 2-tailed vertexes with convex curvature. The curved part of track b is difficult to see, but appears to be parabolic. Track a was measured to be parabolic. a.) (2:O) Fredericks track in Kodak Kodalith type III film. b.) Bardout, *et.al.* track in Kodak Industrex MX125 (double-sided) film.

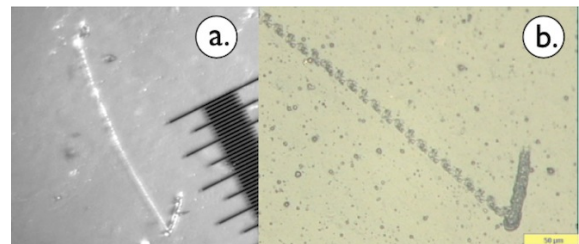## 4. Rodionov and Savvatimova

FIG. 56. a.) (3:O) Fredericks track in Polychrome Litho film. b.) Rodionov and Savvatimova track on Kodak BioMax X-ray film
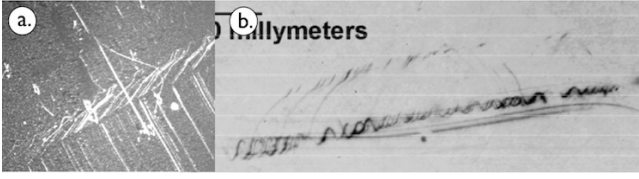
FIG. 57. a.) (1:O) Fredericks track. b.) Rodionov and Savvatimova track.

FIG. 61. (1:O) Fredericks track in Polychrome Litho film. Note similarity to the border structure of 60 and similarity of structure of far right side of track to structures in Fig. 62a.
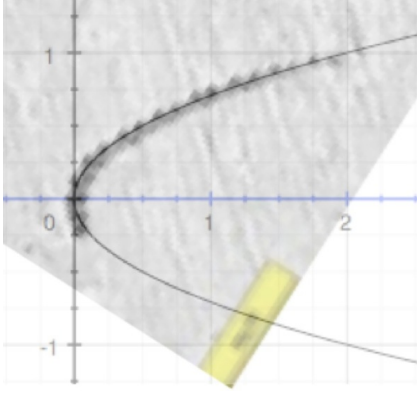
5. Priem, *et.al.*

FIG. 58. Rodionov and Savvatimova track in Palladium electrode showing parabolic curvature. Visual fit to parabola with quadratic equation $x = 2y^2$
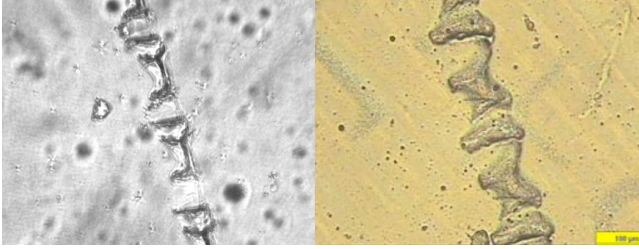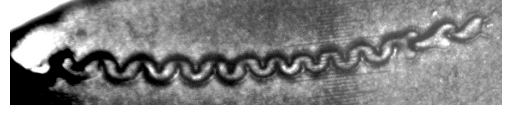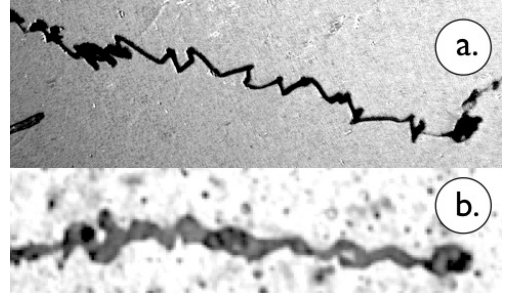

FIG. 62. a.) (1:O) Fredericks track in Polychrome Litho film similar to tracks in section II J. b.) Priem, *et.al.* track showing similarity to Fredericks random type track in a and also to far right side of Fredericks track in 61.
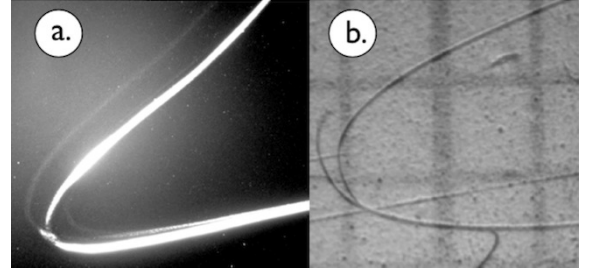

FIG. 59. a.) (3:O) Fredericks track on Polychrome litho film. b.) Rodinov and Savvatimova periodic structure track on nuclear emulsion. Note similarity to Fredericks track where "hourglass" structures are separated by flat structures.

FIG. 63. a.) (2:O) Fredericks track (see also Fig. 23 b.) Priem, *et.al.* track. On both tracks, parabolic curvature and splitting are seen.

FIG. 60. Rodionov and Savvatimova "sausage" track. Note similarity of border structure to Fig. 61.
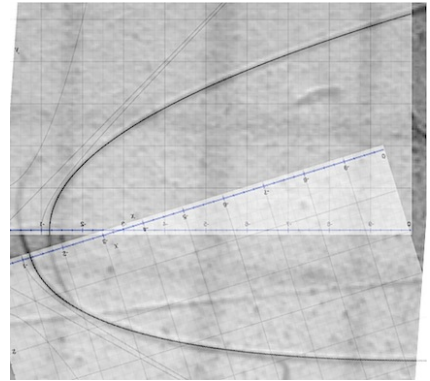

FIG. 64. Priem, *et.al.* track with visual fit to $x = y^2$ parabolas overlaid.

Priem, *et.al.* misidentifies parabolic curvature as circular curvature[6] (translated from French). Until only recently we had similarly misinterpreted parabolic curvature as circular curvature.

> Magnetic monopoles in a fixed electric field perpendicular to the photographic plate, describe circular paths, in the same manner as electric charge describing a circle in a fixed magnetic field perpendicular to its path.

In a bradyonic frame f, a perpendicular applied electric field is expected to produce circular curvature for a magnetic monopole, but the curvature appears to be an exact fit to parabolas in both curves as seen in the image. Further inference is not possible as a diagram of the experimental setup is not included.

FIG. 66. Adamenko and Vysotskii track evaporated in MDS showing parabolic curvature. Visual fit to parabola with quadratic equation $x = y^2$.

6. Adamenko and Vysotskii

The study by Adamenko and Vysotskii provides tracks in MDS rather than photographic emulsions and along with tracks burned into palladium electrodes in studies by Rodionov and Savvatimova, provides insight into the types of energies that are possible with these particles.

It is clear that this track shown by Adamenko and Vysotskii corresponds with all of the periodic tracks in photographic emulsions in that both repeated elements are shown as well as translational symmetry between elements of the two co-terminating tracks as we have seen also in Fig. 17.

FIG. 67. Adamenko and Vysotskii track evaporated in MDS showing parabolic curvature. Detail of track using high magnification. Note similarity to Fig. 17
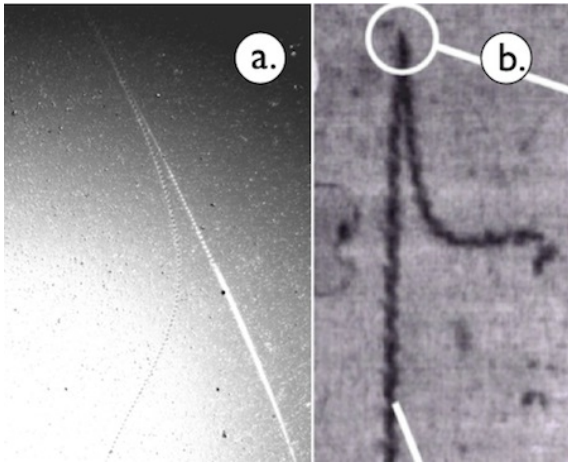
FIG. 65. a.) (3:O) Fredericks track showing co-termination in classical 2-tailed conformation. Track in Kodak Kodalith type III. b.) Adamenko and Vysotskii track evaporated in MDS showing co-termination.
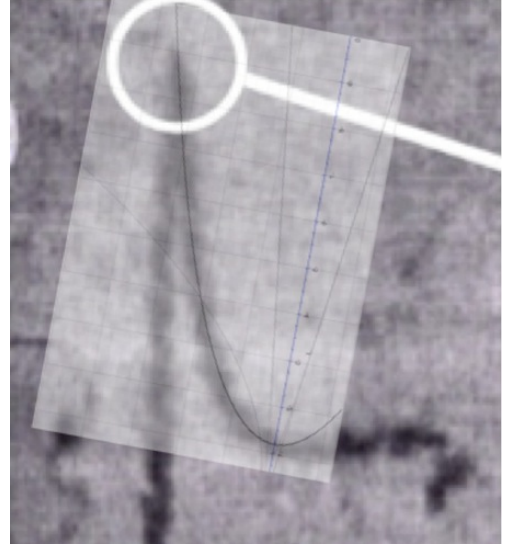
[1] K. A. Fredericks, "Sources and Detection Methods for Tachyons," (1980), unpublished speculations on tachyons; "Investigation of a New Effect Yielding Macroscopic Tracks of Developed Silver in Monodisperse Photographic Emulsions," (1980), unpublished reporting of original effect; "Unidentified Tracks of Developed Silver in Photographic Emulsions: Do These Tracks Correspond to Tachyon Trajectories?" (1997), unpublished overview of all studies until 1997; "Unidentified Tracks of Developed Silver in Photographic Emulsions: Recognition and Categorization," (2001), unpublished review of all studies until 2001. Superseded by current paper.

[2] L. I. Urutskoev, V. I. Liksonov, and V. G. Tsinoev, Ann. Fond. L. de Broglie **27**, 701 (2002); ArXiv Physics e-prints (2001), arXiv:physics/0101089.

[3] L. I. Urutskoev, Ann. Fond. L. de Broglie **29**, 1149 (2004).

[4] N. G. Ivoilov, Ann. Fond. L. de Broglie **31**, 115 (2006).

[5] N. G. Ivoilov and L. I. Urutskoev, Ann. Fond. L. de Broglie **29**, 1177 (2004).

[6] D. Priem *et al.*, Ann. Fond. L. de Broglie **34**, 103 (2009).

[7] G. Bardout, G. Lochak, and D. Fargueb, Ann. Fond. L. de Broglie **32**, 551 (2007).

[8] V. Adamenko and V. I. Vysotskii, in *Proceedings of the 14th International Conference on Condensed Matter Nuclear Science and the 14th International Conference on Cold Fusion (ICCF-14) 10-15 August 2008 Washington DC*, edited by D. J. Nagel and M. E. Melich (New Energy Foundation, Inc., 2008) p. 484.

[9] S. V. Adamenko and V. I. Vysotskii, Ann. Fond. L. de Broglie **33**, 13 (2008).

[10] B. Rodionov and I. Savvatimova, "Unusual structures on the material surfaces irradiated by low energy ions," in *Condensed Matter Nuclear Science* (2005) Chap. 44, pp. 421–429.

[11] I. Savvatimova and J. Dash, in *The 9th International Conference on Cold Fusion, Condensed Matter Nuclear Science. 2002. Tsinghua Univ., Beijing, China*, edited by Z. Z. Li (Tsinghua Univ. Press, 2002).

[12] V. D. Kuznetsov, G. V. Mishinsky, F. M. Penkov, V. I. Arbuzov, and V. I. Zheminik, Ann. Fond. L. de Broglie **28**, 173 (2003).

[13] G. V. Mishinsky and V. D. Kuznetsov, Ann. Fond. L. de Broglie **33**, 331 (2008).

[14] G. Lochak, Z. Naturforsch. **A62**, 231 (2007), arXiv:0801.2752 [quant-ph].

[15] D. Priem *et al.*, Ann. Fond. L. de Broglie **33**, 129 (2008).

[16] G. Lochak, personal communication.

[17] C. Schneider, W. Rasband, and K. Eliceiri, Nat. Methods **9**, 671 (2012).

[18] G. Lochak and L. Urutskoev, in *Condensed Matter and Nuclear Science (Proceedings of the 11th International Conference on Cold Fusion, 31 October-5 November, Marseille, France, 2004)*, edited by J. Biberian (World Scientific, 2006) p. 421.

[19] R. Mignani and E. Recami, Lett. Nuovo Cimento **9**, 367 (1974).

[20] L. Parker, Phys. Rev. **188**, 2287 (1969).

[21] D. Weingarten, Ann. Phys. **76**, 510 (1973).

[22] E. Recami and R. Mignani, Nuovo Cimento **4**, 209 (1974).

[23] E. Recami, Nuovo Cimento **9**, 1 (1986), 10.1007/BF02724327.

[24] C. F. Powell, *The study of elementary particles by the photographic method* (Pergamon Press, London, 1959).

[25] W. H. Barkas, *Nuclear Research Emulsions: Techniques and theory*, Pure and applied physics (Academic Press, New York, 1963).

[26] Fig. 6 shows one image of a track consistent with delta rays in the entire study. It is interesting to note also that this track and others in this exposure are *reversed* tracks. (see Section II H).

[27] H. D. Ables, AAS Photo-Bull. **3**, 18 (1971); T. A. Babcock, **13**, 6 (1976); W. C. Miller, Publ. Astron. Soc. Pac. **76**, 328 (1964); T. M. Muliarchik and K. I. Petrova, Sov. Astron. **1**, 108 (1957).

[28] Lith development refers generally to low-sulfite, formaldehyde-hydroquinone type developers which tend to develop surface latent image. Solution physical development refers to developers that tend to work by dissolving part of the silver halide grain, putting the Ag^+ ions into solution and potentially plating complexed Ag^0 onto the latent image. Solution physical developers will activate internal as well as surface latent images. This may be important to distinguish between certain types of radiation. X-rays and higher energies penetrate AgBr grains and will create internal latent images whereas visible light tends to create mainly surface latent images.

[29] Monodisperse emulsions have all AgBr grains of a similar size and are generally finer grained, less sensitive to light and higher contrast while polydisperse emulsions have a wide range of AgBr grain sizes, are relatively coarser grained, more sensitive to light with a lower contrast.

[30] T. H. James, *The Theory of the photographic process, Fourth Ed.* (Macmillan, New York, 1977).

[31] *Biological Imaging Applications - Technical Note P-64, Kodak Products for Light Microscope Autoradiography*, Eastman Kodak Co., Rochester, New York (1987).

[32] R. Katz and D. R. Parnell, Phys. Rev. **116**, 236 (1959).

[33] T. E. Furtak and R. Katz, Radiat. Eff. **11**, 195 (1971).

[34] G. R. Carruthers, AAS Photo Bulletin **5**, 3 (1972).

[35] R. Katz and E. J. Kobetich, Phys. Rev. **186**, 344 (1969).

[36] J. Rotblat and C. T. Tai, Nature **164**, 835 (1949).

[37] J. Beringer *et al.* (Particle Data Group), Phys. Rev. D **86**, 010001 (2012).

[38] P. Fraundorf, "A conservation-law view of everyday motion," (2007), department of Physics and Astronomy and Center for NanoScience at the University of Missouri in Saint Louis.

[39] D. E. Groom, Phys. Rep. **140**, 323 (1986).

[40] G. Giacomelli, S. Manzoor, E. Medinaceli, and L. Patrizii, J.Phys.Conf.Ser. **116**, 012005 (2008), arXiv:hep-ex/0702050 [HEP-EX].

[41] W. Braunschweig *et al.*, Z. Phys. C **38**, 543 (1988), 10.1007/BF01624358.

[42] T. Gentile *et al.*, Phys. Rev. D **35**, 1081 (1987).

[43] A. Abulencia *et al.* (CDF Collaboration), Phys. Rev. Lett. **96**, 201801 (2006).

[44] "A direct search for dirac magnetic monopoles," (2004), the CDF Collaboration 2004, CDF note 7183.

[45] A. Aktas *et al.* (H1 Collaboration), Eur. Phys. J. **C41**, 133 (2005), arXiv:hep-ex/0501039 [hep-ex].

[46] O. Heaviside, *Electrical Papers*, Vol. 2 (Macmillan and Co., New York, 1894) p. 494.

[47] A. Sommerfeld, K. Acad. Wet. Amsterdam Proc. **8**, 346 (1904).

[48] This paradox, which has been solved,[74] showed how faster-than-light particles allowed the sending of information into the past.

[49] O. M. P. Bilaniuk, V. K. Deshpande, and E. C. G. Sudarshan, Am. J. Phys. **30**, 718 (1962).

[50] Y. P. Terletskii, Sov. Phys. Dok. **5**, 784 (1961).

[51] S. Tanaka, Progr. Theor. Phys. **24**, 177 (1960).

[52] G. Feinberg, Phys. Rev. **159**, 1089 (1967).

[53] G. Feinberg, Sci. Am. **219**, 69 (1968).

[54] E. Recami, ArXiv e-prints (2008), arXiv:0804.1502 [physics.class-ph].

[55] E. Recami *et al.*, *Tachyons, Monopoles and Related Topics*, edited by E. Recami (North-Holland, Amsterdam, 1978).

[56] $B = \mu_m H$ with $\mu = \mu_m = K_m \mu_0$, where μ_0 is magnetic permeability of space and K_m is the relative permeability of the material.

[57] M. Fayngold, Teor. Mat. Fiz. **47**, 395 (1981).

[58] A. E. Everett, Phys. Rev. D **13**, 795 (1976).

[59] M. Davidson, Phys. Essays **14**, 66 (2001), arXiv:quant-ph/0203053 [quant-ph].

[60] M. Fayngold, *Special Relativity and Motions Faster than Light* (Wiley-VCH Verlag GmbH, Weinheim, 2002).

[61] M. D'Angelo, Y.-H. Kim, S. P. Kulik, and Y. Shih, Phys. Rev. Lett. **92**, 233601 (2004), arXiv:quant-ph/0401007.

[62] R. Fox, Phys. Rev. D **5**, 329 (1972).

[63] M. Fayngold, ArXiv e-prints (2011), arXiv:1104.2531 [physics.gen-ph].

[64] J. Soucek, eprint arXiv:quant-ph/0107040 (2001), arXiv:arXiv:quant-ph/0107040; eprint arXiv:quant-ph/0404094 (2004), arXiv:arXiv:quant-ph/0404094; In: Jarolm Bure and Vladimr Soucek (eds.): Proceedings of the Winter School "Geometry and Physics". Circolo Matematico di Palermo, Palermo, 1989. Rendiconti del Circolo Matematico di Palermo, Serie II, Supplemento No. 21. pp. [325]–341. (1989).

[65] M. P. Davidson, (2001), arXiv:quant-ph/0103143 [quant-ph].

[66] R. Tomaschitz, Int. J. Mod. Phys. D **7**, 279 (1998).

[67] A. Barut, G. Maccarrone, and E. Recami, Nuovo Cimento A **71**, 509 (1982), 10.1007/BF02770989.

[68] M. Ibison, ArXiv e-prints (2007), arXiv:0704.3277 [physics.gen-ph].

[69] U. Jentschura and B. Wundt, (2012), arXiv:1205.0521 [hep-ph]; E. Trojan, (2012), arXiv:1204.1370 [hep-ph].

[70] C. Schwartz, J. Math. Phys. **52**, 052501 (2011), arXiv:1011.4847 [math-ph].

[71] E. Recami and G. Maccarrone, Lett. Nuovo Cimento **37**, 345 (1983), 10.1007/BF02887015.

[72] W. F. Berg, Photogr. J. **96B**, 154 (1946); G. S. Moore, **81**, 27 (1941); A. Guttman, Photogr. Sci. Eng. **12**, 146 (1968); G. C. Farnell and P. G. Powell, Photogr. Sci. **11**, 57 (1963); J. C. Marchant, J. Opt. Soc. Am. **54**, 768 (1964).

[73] A. Beiser, Rev. Mod. Phys. **24**, 273 (1952).

[74] E. Recami, Lett. Nuovo Cim. **44**, 587 (1985), arXiv:hep-th/9508164 [hep-th].